

## Journal Pre-proofs

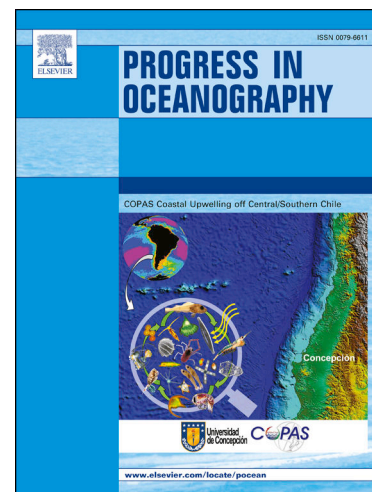
Net community oxygen production derived from Seaglider deployments at the Porcupine Abyssal Plain site (PAP; northeast Atlantic) in 2012-13

U. Binetti, J. Kaiser, G.M. Damerell, A. Rummyantseva, A.P. Martin, S. Henson, K.J. Heywood

PII: S0079-6611(20)30031-8  
DOI: <https://doi.org/10.1016/j.pocean.2020.102293>  
Reference: PROOCE 102293

To appear in: *Progress in Oceanography*

Received Date: 30 April 2019  
Revised Date: 18 December 2019  
Accepted Date: 4 February 2020



Please cite this article as: Binetti, U., Kaiser, J., Damerell, G.M., Rummyantseva, A., Martin, A.P., Henson, S., Heywood, K.J., Net community oxygen production derived from Seaglider deployments at the Porcupine Abyssal Plain site (PAP; northeast Atlantic) in 2012-13, *Progress in Oceanography* (2020), doi: <https://doi.org/10.1016/j.pocean.2020.102293>

This is a PDF file of an article that has undergone enhancements after acceptance, such as the addition of a cover page and metadata, and formatting for readability, but it is not yet the definitive version of record. This version will undergo additional copyediting, typesetting and review before it is published in its final form, but we are providing this version to give early visibility of the article. Please note that, during the production process, errors may be discovered which could affect the content, and all legal disclaimers that apply to the journal pertain.

Net community oxygen production derived from Seaglider deployments at the Porcupine Abyssal Plain site (PAP; northeast Atlantic) in 2012-13

U. Binetti<sup>1,2</sup>, J. Kaiser<sup>2</sup>, G. M. Damerell<sup>2</sup>, A. Rumyantseva<sup>3</sup>, A.P. Martin<sup>4</sup>, S. Henson<sup>4</sup>, K. J. Heywood<sup>2</sup>

<sup>1</sup>Centre for Environment, Fisheries and Aquaculture Science, Lowestoft, UK

[Umberto.binetti@cefas.co.uk](mailto:Umberto.binetti@cefas.co.uk), [u.binetti@uea.ac.uk](mailto:u.binetti@uea.ac.uk)

Umberto Binetti, Cefas Laboratories, Pakefield Road, Lowestoft, UK NR33 0HT.

<sup>2</sup>Centre for Ocean and Atmospheric Sciences, School of Environmental Sciences, University of East Anglia, Norwich, United Kingdom

<sup>3</sup>School of Ocean and Earth Sciences, University of Southampton, Southampton, UK

<sup>4</sup>National Oceanography Centre, Southampton, UK

## Abstract

As part of the OSMOSIS project, a fleet of gliders surveyed the Porcupine Abyssal Plain site (Northeast Atlantic) from September 2012 to September 2013. Salinity, temperature, dissolved oxygen concentration and chlorophyll fluorescence were measured in the top 1000 m of the water column. Net community production ( $N$ ) over an annual cycle using an oxygen-budget approach was compared to variations of several parameters (wind speed, mixing layer depth relative to euphotic depth, temperature, density, net heat flux) showing that the main theories (Critical Depth Hypothesis, Critical Turbulence Hypothesis, Heat-flux Hypothesis) can explain the switch between net heterotrophy to net autotrophy in different times of the year. The dynamics leading to an increase in productivity were related to shifts in regimes, such as the possible differences in nutrient concentration. The oxygen concentration profiles used for this study constitute a unique dataset spanning the entire productive season resulting in a data series longer than in previous studies. Net autotrophy was found at the site with a net production of  $(6.4 \pm 1.9)$  mol m<sup>-2</sup> in oxygen equivalents (or  $(4.3 \pm 1.3)$  mol m<sup>-2</sup> in carbon equivalents). The period exhibiting a deep chlorophyll maximum between 10 m and 40 m of depth contributed  $(1.5 \pm 0.5)$  mol m<sup>-2</sup> in oxygen equivalent to the total  $N$ . These results are greater than most previously published estimates.

## Keywords

Dissolved Oxygen, Biological production, Algal bloom, Ocean-Atmosphere System, North Atlantic, Porcupine Abyssal Plain, Gliders

## Highlights

- The area analysed is autotrophic over an annual cycle

- Marine net biological production is estimated at  $19 \text{ mmol m}^{-2} \text{ d}^{-1}$  in  $\text{O}_2$  equivalents with a total production of  $6.4 \text{ mol m}^{-2} \text{ O}_2$  equivalent
- Initiation of phytoplankton blooms in different time of the year follow dynamics described by up to three theories (Critical Depth Hypothesis, Critical Turbulence Hypothesis, Heat-flux Hypothesis).
- Water is oxygen undersaturated during the whole winter period.

## 1 Introduction

Marine net biological production ( $N$ ) is the balance between oxygen ( $\text{O}_2$ ) production by phytoplankton during photosynthesis and  $\text{O}_2$  consumption during respiration by the entire marine community. The seas around the world harbour almost half of the global plant production (Field et al, 1998; Williams, 1998), moving carbon and oxygen within and across compartments and reservoirs. By causing supersaturation or undersaturation of surface waters, biota is able to drive fluxes between the ocean and the atmosphere. This makes the ocean a carbon sink or a source depending on biological activity, which is important for estimating the global carbon budget and understanding how  $\text{CO}_2$  influences climate as a greenhouse gas (Falkowski, 1998).

Measurement of  $N$  over the entire annual cycle are important to understand the metabolic balance of the open ocean (i.e., the sign and magnitude of  $N$ ), which is the focus of a long-running debate (del Giorgio et al., 1997; Duarte and Agustí, 1998; Williams 1998; Duarte et al., 1999; Williams and Bowers, 1999; del Giorgio and Duarte, 2002; Karl et al., 2003; Hansell et al., 2009; Ducklow and Doney, 2013; Williams et al., 2013; Duarte et al, 2013). Uncertainty about  $N$  derives from the use of different methods for the calculation of  $N$  and its components. Several biases are known to affect *in vitro* measurements and their comparability with the real ocean (Williams et al., 1998; Kaiser et al., 2005). There are also challenges in separating the influence of biological and physical processes on *in situ* measurements (Hamme and Emerson, 2006; Emerson et al., 2008). It is not even clear what some of the methods used are actually measuring (Regaudie-de-Gioux et al., 2014).

The analysis of  $N$  variations within the annual cycle, and their comparison with variations in other parameters, are instead useful to understand what factors are limiting or stimulating production and to investigate the validity of different mechanisms proposed so far. In regimes of nutrient limitation, gradual deepening of the mixed layer into nutrient-rich waters has been recognised as a plausible explanation for autumn blooms (Marra et al., 1990; Findlay et al., 2006). More recently, productivity peaks have been related to pulses of nutrients created by the interaction between wind and surface currents (Rumyantseva et al., 2015). The discussion about what triggers autotrophy when nutrients are not limited is more complicated. The Sverdrup Hypothesis (Critical Depth Hypothesis or CDH, Sverdrup, 1953) sees light as a driving factor: the plankton community is productive when the mixed layer is shallower than the critical depth, which is the depth above which total production exceeds total respiration. Since 1953, a long discussion has flourished to confirm or refute the Sverdrup CDH and new hypotheses have been proposed based on its weak points such as the assumption of phytoplankton behaving as a passive tracer. New hypotheses focus on the influence that turbulence has on the ability of the phytoplankton to access light. According to the Critical Turbulence

Hypothesis (CTH, Huismann, 1999), high turbulence displaces the plankton at a faster rate than its growth rate. When turbulence decreases below a critical value, plankton grows faster than it is displaced and this leads to blooms (i.e., accumulation of oxygen and chlorophyll at the surface). Taylor and Ferrari (2011) linked the turbulence to the net heat flux, suggesting that the inversion from negative heat flux (water cooling) to positive heat flux (water warming) and the consequent shut down of convective mixing is a reliable parameter to predict the start of the bloom on an interannual timescale (Heat Flux Hypothesis or HFH). Enriquez and Taylor (2015) proposed another model linking the variations in turbulence induced by wind stress and water cooling (negative net heat flux leading to convective mixing) to the depth of the mixing layer. They predicted that when the mixing layer shoals, the phytoplankton respond with an increased growth rate (and then increased production). Behrenfeld (2010) suggested the Recoupling-Dilution Hypothesis, according to which phytoplankton has a positive growth rate when the mixed layer is deepening because of lower predation pressure.

The first goal of the present study is to estimate the magnitude of  $N$  in the productive layer of the water column through the analysis of variations of the oxygen inventory over time, based on oxygen concentration measured *in situ* by underwater gliders. Thanks to the high frequency of glider measurements and considering the length of this time series, the present study tries to overcome limitations in calculating  $N$  due to low spatial or temporal resolution. The present study surveyed an area located in the North Atlantic, in the proximity of the frequently sampled Porcupine Abyssal Plain (PAP) Sustained Observatory. This allows us to compare  $N$  estimates with results of previous studies that focused on the same area (e.g., Körtzinger et al., 2008a; Frigstad et al., 2015) along with basin-wide estimates. Furthermore, the availability of a suite of different parameters provided insights into the mechanisms that trigger increases in production. The second aim of the paper is to compare variations in  $N$  with other parameters to understand how observation fit with the different theories suggested to explain the increase in productivity.

## 2 Material and methods

### 2.1 Data acquisition

The OSMOSIS project included five cruises and three glider missions performed at PAP (Figure 1) between September 2012 and September 2013. The cruises enabled the deployment and recovery of the gliders and the collection of a suite of *in situ* parameters to be used for calibration of the glider data. The three glider missions were carried out with short overlapping periods when the research vessels visited the area to swap gliders. Details of the glider campaigns, quality control, calibration and analysis of the physical oceanographic context of the year-long time series are provided by Damerell et al. (2016). During each mission two gliders operated at the same time moving along two separate butterfly- (or hourglass-) shaped transects oriented perpendicular to each other (one glider moving north-south and the other east-west) centred around 48.7° N and 16.2° W with 15 km long edges (Figure 1). Because of a malfunctioning oxygen sensor and deviations from the designated transect, only one glider per mission was used to create the year-long dataserie. Data from glider SG566 were considered between September 2012 and January 2013; SG502 between January 2013 and April 2013 and

SG566 a second time between April 2015 and September 2015. The glider data are held at the British Oceanographic Data Centre and can be accessed at <https://doi.org/10/cqc6>.

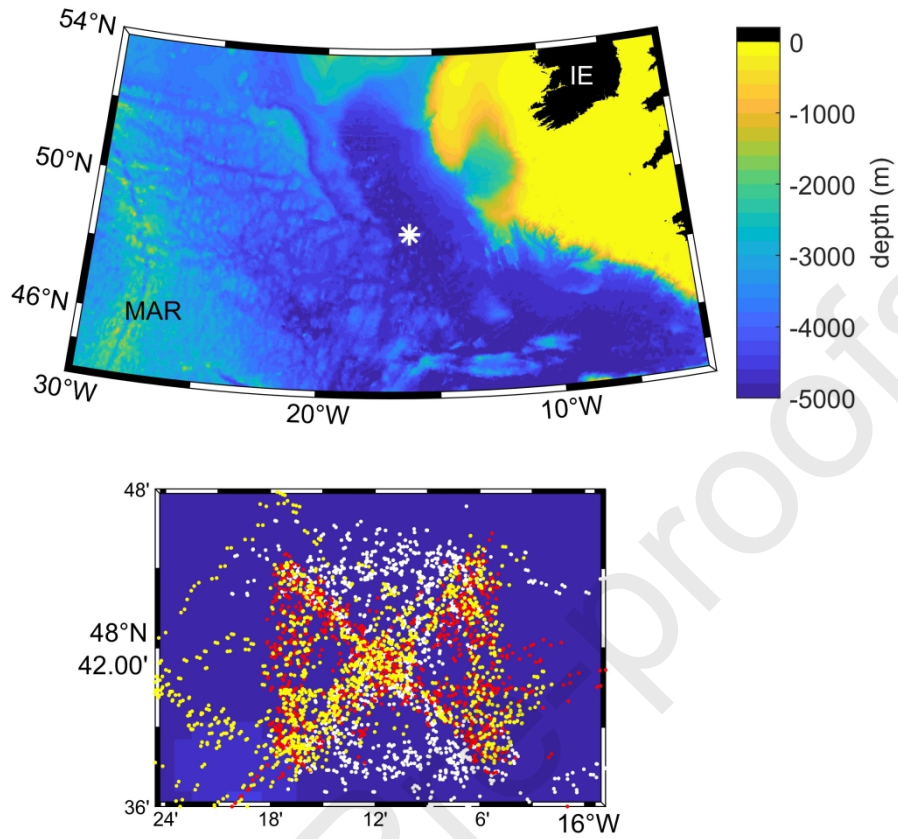


Figure 1 Survey Location by the Porcupine Abyssal Plain Sustained Observatory. Top panel: survey location compared with ocean floor bathymetry. Bottom panel: butterfly/hourglass paths described by gliders during the missions; point represent surfacing location of gliders: white is SG566 (first mission), red is SG502 and yellow is SG566 (second mission).

## 2.2 CTD calibration

The calibration of the data followed several steps. Ship-CTD oxygen concentration,  $c(\text{O}_2)$ , profiles were calibrated against water samples analysed by Winkler titration. Glider  $c(\text{O}_2)$  profiles were first adjusted to account for the response time of the optodes and subsequently calibrated against the Winkler-calibrated ship-CTD  $c(\text{O}_2)$  profiles.

CTD casts were performed just before the deployment of the gliders and soon after their recovery. Oxygen concentration was measured by a Clark-type electrode (Seabird SBE43) attached to the rosette frame and water was sampled by the means of Niskin bottles attached to the same rosette. At the end of the cast, Winkler samples were collected from selected Niskin bottles and their  $c(\text{O}_2)$  was measured by Winkler titration following WOCE protocols (Culbertson 1991; Dickson, 1996). For each cast, CTD  $c(\text{O}_2)$  was calibrated by linear regression against Winkler-derived  $c(\text{O}_2)$ .

## 2.3 Response time correction

The gliders recorded  $c(\text{O}_2)$  by means of optodes (Aanderaa Data Instruments; Tengberg et al., 2003), which measure the lifetime of the red light emitted by excited porphyrins in a sensing foil as a temperature-

compensated phase difference ( $\phi_{TC}$ ), which depends on the  $c(O_2)$ . The diffusion time of the gas through the optode foil is characterised by a certain response time ( $\tau$ ). When plotting  $\phi_{TC}$  against pressure, the response time shifts  $\phi_{TC}$  profiles in the same direction the glider is moving in. Gradients will appear deeper than their actual depth when gliders descend and shallower when gliders ascend through the water column. A best-fit response time ( $\tau$ ) was determined from each pair of consecutive ascents and descents over the top 300 m. All response times of ascent-descent pairs in the same glider mission were fitted to a normal distribution and its central value was used as  $\tau$  to shift all the profiles of the same glider mission. The best-fit response times were applied to shift the profiles backwards in time, which resulted in a shift of the descent profiles upwards and the ascent profiles downwards. Variations and uncertainty in  $\tau$  may be caused by variations in temperature and short-term changes in the vertical  $c(O_2)$  profile during subsequent glider dives.

## 2.4 Glider calibration and despiking

The  $\tau$ -corrected  $\phi_{TC}$  profiles were calibrated using the Winkler-calibrated ship-CTD  $c(O_2)$  profiles, using the closest CTD cast (less than 4 km and less than 3 h away).  $\phi_{TC}$  profiles from several glider dives and several CTD profiles were used in the calibration as long as the glider and the ship were within the limits of proximity defined above.

Calibrated phase differences  $\phi_{cal}(\text{ship-CTD})$  were calculated from ship-CTD  $c(O_2)$  as follows:

- 1) calculate water vapour pressure  $p_{vap}$  using potential temperature and practical salinity;
- 2) calculate oxygen saturation concentration  $c_{sat}(O_2)$  using the parameterisation of Garcia and Gordon (1992) with the solubility coefficients of Benson and Krause (1984);
- 3) calculate air saturation  $s(O_2)$  equivalent to an atmospheric pressure of 1013.25 hPa where  $s(O_2) = c(O_2) / c_{sat}(O_2)$ ;
- 4) calculate partial pressure of oxygen,  $\Delta p(O_2)$ , using  $s(O_2)$  and  $p_{vap}$
- 5) calculate  $\phi_{cal}$  by inverting the manufacturer-provided sensing-foil specific polynomial that uses temperature,  $\Delta p(O_2)$  and 21 coefficients ( $A_0$  to  $A_{13}$  and  $B_0$  to  $B_6$ ) to derive  $\phi_{cal}$

$\phi_{cal}(\text{ship-CTD})$  profiles and glider  $\phi_{TC}$  profiles were then binned according to potential density and compared. The offset and slope of their linear regression was used as  $C_0$  and  $C_1$  in Eq. 1:

$$\phi_{cal}(\text{glider}) = C_0 + C_1 \phi_{TC} \quad (\text{Eq. 1})$$

Since CTD casts were performed during the cruises at the deployment and recovery of the gliders, there was a linear calibration equation obtained at the beginning and at the end of each mission. In case the two calibration equations were not the same (indicating drift of the sensor over time), a time-varying  $C_0$  and  $C_1$  was calculated for each dive interpolating over time between the values at the beginning and end of each mission. Each dive had therefore a unique calibration equation that transformed  $\phi_{TC}$  into  $\phi_{cal}$ .



$\phi_{\text{cal}}(\text{glider})$  profiles were then transformed into calibrated glider  $c(\text{O}_2)$  with the same five steps used for the back-calculation of the CTD  $\phi_{\text{cal}}$  in reverse order.

Spikes in the profiles were automatically flagged when a data point matched any of the following criteria:

- 1) unrealistic  $c(\text{O}_2)$ , i.e. values  $<0 \mu\text{mol kg}^{-1}$  or  $>1000 \mu\text{mol kg}^{-1}$ ;
- 2) significant increase in the standard deviation of a  $c(\text{O}_2)$  profile due to a single point;
- 3) single points with anomalous  $c(\text{O}_2)$  within water masses with constant concentrations;
- 4)  $c(\text{O}_2)$  values apparently above the surface (due to pressure sensor inaccuracies).

Visual despiking of profiles was carried out to remove anomalous  $c(\text{O}_2)$  at the surface due to light hitting the foil, waves that expose the sensor to air or problems in  $\tau$  correction.

At the end of the process, 527 points were flagged as spikes in SG566 (0.14 % of the total), 837 in SG502 (0.22 % of the total) and 546 in the second SG566 mission (0.14% of the total). All these spikes were in the upper 40 m of the water column. The uncertainty associated with the calibration of  $c(\text{O}_2)$  values is expressed as the standard deviation of the residual difference between ship-CTD  $c(\text{O}_2)$  and glider  $c(\text{O}_2)$  after the calibration. The uncertainty for the whole dataset was computed as the mean of the uncertainties of the six different calibrations (one at the beginning and one at the end of each mission,  $2.2 \mu\text{mol kg}^{-1}$ ). With the uncertainty in the ship-CTD calibration against Winkler samples of  $1.6 \mu\text{mol kg}^{-1}$ , the overall uncertainty associated with calibrating glider  $c(\text{O}_2)$  was  $2.7 \mu\text{mol kg}^{-1}$ .

At the end of the calibration, entire profiles were also flagged as anomalous and not considered in further calculations. In particular, the profiles recorded after the 11<sup>th</sup> August 2013 were disregarded because biofouling affected the optode of the SG566. Biofouling was identified by anomalous readings in  $c(\text{O}_2)$  throughout the whole water column and its presence was confirmed by visual inspection when the glider was recovered. More details about biofouling during this survey are provided in Appendix A – Biofouling, including the explanation of why the 11<sup>th</sup> August was chosen as cut-off date.

## 2.5 Mixed layer calculation

The calculation of  $z_{\text{mix}}$  was performed for each of the 4035  $c(\text{O}_2)$  profiles of the OSMOSIS time series using three consecutive glider missions (one glider per mission).  $c(\text{O}_2)$  at 5 m depth (calculated by interpolation) was used as reference concentration,  $c_{\text{ref}}(\text{O}_2)$ , which is the estimate of  $c(\text{O}_2)$  in the mixed layer. This depth is shallower than the one (10 m) chosen in previous studies (e.g. de Boyer Montégut et al., 2004, Castro-Morales and Kaiser, 2012), using the high-resolution data available all the way to the surface. Shallower depths were not considered because of noisiness of data in the very first metres of the water column. For 25 profiles the interpolation was not possible because their shallowest data-point was deeper than 5 m. For these profiles, the shallowest data-point of the profile was used as  $c_{\text{ref}}(\text{O}_2)$ . For 51 profiles the shallowest data point was deeper than 10 m; for these profiles  $c_{\text{ref}}(\text{O}_2)$  and  $z_{\text{mix}}$  was not computed.

$c(\text{O}_2)$  profiles were smoothed by a local regression method using weighted linear least squares and a first degree polynomial model to eliminate possible effects of noise on the calculation. Forty random profiles with an obvious mixed layer were selected throughout the whole year and visually inspected to choose a threshold relative  $\text{O}_2$  concentration change of 0.5 %. This threshold is also in accordance with the one used for similar calculations by Castro-Morales and Kaiser (2012). Lower thresholds would result in random  $z_{\text{mix}}(\text{O}_2)$  values not corresponding to a significant difference from  $c_{\text{ref}}(\text{O}_2)$ . The use of higher threshold would instead result in estimates of the mixed layer deeper than the actual layer visible in the profiles.

For each smoothed profile, the shallowest depth at which  $|\Delta c|/c_{\text{ref}}$  (Eq. 3) exceeded 0.005 was considered to be  $z_{\text{mix}}(\text{O}_2)$

$$|\Delta c|/c_{\text{ref}} = |c(\text{O}_2) / c_{\text{ref}}(\text{O}_2) - 1| \quad (\text{Eq. 3})$$

## 2.6 Production calculation

Marine biological production ( $N$ ) at the top of the water column was calculated analysing the changes in the oxygen inventory per unit area ( $I$ ). Only the  $c(\text{O}_2)$  profiles from glider descents were used for productivity calculations because some of the ascents were affected by spikes caused by sunlight hitting the optode foil near the surface (see Appendix A). The calculations focused on the top 60 m ( $z_{\text{lim}}$ ) of the water column, which was equivalent to the mean euphotic depth ( $z_{\text{eup}}$ ) of  $(60 \pm 15)$  m during the study.  $z_{\text{eup}}$  was defined as the depth at which PAR falls to 1% of the level measured at the surface. PAR was measured in situ by sensor installed on the seagliders.

$N$  was calculated as

$$N = \Delta I / \Delta t + F_{\text{as}} - E \quad (\text{Eq. 4})$$

where  $F_{\text{as}}$  is the air-sea  $\text{O}_2$  flux (positive for  $\text{O}_2$  outgassing),  $E$  is entrainment and  $N$  is net community production.  $\Delta I$  was calculated as the  $c(\text{O}_2)$  inventory change above  $z_{\text{lim}}$  between consecutive profiles. Profile inventory was calculated by integrating  $c(\text{O}_2)$  over depth.

$F_{\text{as}}$  was calculated using the correction for bubble injection ( $\Delta$ ) formulated by Woolf and Thorpe (1991):

$$F_{\text{as}} = k(\text{O}_2)[c(\text{O}_2) - (1 + \Delta)c_{\text{sat}}(\text{O}_2)] \quad (\text{Eq. 5})$$

where  $k(\text{O}_2)$  is gas transfer velocity for oxygen;  $c(\text{O}_2)$  is the dissolved oxygen concentration in the mixed layer; and  $c_{\text{sat}}(\text{O}_2)$  is the oxygen saturation concentration calculated according to the Benson and Krause (1984) fit of Garcia and Gordon (1992) using the atmospheric pressure derived by interpolation of ERA-Interim reanalysis data (<http://www.ecmwf.int/en/research/climate-reanalysis/era-interim>, resolution of 6 hours and  $0.125^\circ$  in latitude and longitude).  $c(\text{O}_2)$  and  $c_{\text{sat}}(\text{O}_2)$  used to calculate  $F_{\text{as}}$  were derived from the mean value for the top 10 m or as the mean above  $z_{\text{mix}}$  when  $z_{\text{mix}} < 10$  m. The gas transfer velocity at a Schmidt number  $Sc = 600$  was parameterised following Nightingale et al. (2000) using the daily averaged wind speed at 10 m derived from ERA-Interim reanalysis with the same resolution as the atmospheric pressure.  $F_{\text{as}}$  used to calculate  $N$  between



two profiles was the mean of the  $F_{as}$  measured for these two profiles. It is worth noting that Song et al. (2013) compared ERA-Interim data with measurements from eight buoys, showing a good agreement between re-analysis and in situ measurements (regression coefficients for wind speed was above 0.7 and for direction was greater than 0.79). However, ERA-Interim overestimated wind data at the buoy stations, with the max difference of 1.8 m/s; and 13% ERA-Interim wind data below 6 m/s were flagged as not good. There is therefore the possibility that  $F_{as}$  used here might be slightly overestimated.

Entrainment was considered as the change of  $c(O_2)$  due to deep water mixed all the way to the surface in the mixed layer when  $z_{mix}$  deepens. Entrainment could be positive or negative, corresponding to an increase or a decrease of the oxygen inventory.  $E$  between any two profiles at times  $t_1$  and  $t_2$  was considered only when  $z_{mix}$  deepened and when  $z_{mix}$  at  $t_2$  was deeper than  $z_{lim}$ . Otherwise,  $E$  was equal to zero, e.g. when  $z_{mix}$  deepened, but remained above  $z_{lim}$ , a redistribution of the oxygen was assumed without any  $O_2$  flux occurring through  $z_{lim}$  and therefore no variation in the oxygen inventory above  $z_{lim}$  ( $I(z_{lim})$ ). In order to calculate  $z_{mix}$  deepening and shoaling,  $z_{mix}$  values were smoothed using a moving filter with 5 points span.

This was an Eulerian rather than Lagrangian study and therefore part of  $\Delta I$  between adjacent profiles was the signal of geographical heterogeneity (patchiness) and horizontal advection. Advection has been considered negligible in previous studies (Emerson et al., 2008; Nicholson et al., 2008; Nicholson et al., 2015) due to the rapid effect of air-sea  $O_2$  flux inequibrating the concentration at the surface. However, Alkire et al. (2014) and Hull et al. (2016) showed that advection can significantly affect  $N$  estimates over time scales of days/months and for spatial scales less than 50 km. In this study, in order to consider the effect of advection, the individual  $N$  values measured between consecutive profiles were averaged over 7 days. Looking at the time-series, 7 days was in fact a period longer than the glider took to traverse the distance between large  $N$  values (sign of glider entering a  $O_2$ -rich advected water mass) and large negative  $N$  values (gliders getting out of the advected water mass). Averaging over 7 days was considered therefore an effective way to cancel out the positive and negative contribution of any water mass advected in the area to  $N$  calculation. This is also in line with Alkire et al. (2014), which in a similar glider experiment showed that the time scale of advection processes was around 4 days. In the present study, running averages of  $N$  for overlapping 7 day-long bins were assumed to be a valid estimate of biological activity (sensitivity to averaging period is tested in Appendix B).

The period of 7 days is also the approximate time any glider took to complete its butterfly- or hourglass-shaped transects and the averaging therefore gave estimates of  $N$  for the entire surveyed area, disregarding its internal geographical heterogeneity.

The variation in  $c(O_2)$  were also analysed in relation to the thermal exchange between atmosphere and the ocean. In order to do this, the timeseries of net heat flux ( $H$ ) was obtained from ERA-Interim reanalysis. The resolution of 6 hours and  $0.125^\circ$  in latitude and longitude.

### 3.1 Annual time series

The distribution of oxygen measured by the gliders at PAP between September 2012 and September 2013 is plotted against time and depth in Figure 2, along with oxygen saturation ( $s(\text{O}_2)$ , ratio of  $c(\text{O}_2)$  over  $c_{\text{sat}}(\text{O}_2)$ ) and Apparent Oxygen Utilization (AOU, difference  $c_{\text{sat}}(\text{O}_2) - c(\text{O}_2)$ ). The other physical parameters measured concurrently with  $c(\text{O}_2)$  are shown in Figure 3. The vertical distributions suggest the presence of three layers in the water column. These layers have also been described by Damerell et al. (2016) who analysed salinity and temperature measured concurrently with the oxygen concentrations analysed in the present study. The top layer was roughly 150 m deep. This layer included the ocean surface boundary layer and had a seasonal cycle in the temperature due to solar insolation. Salinity was more variable, it did not follow any seasonal cycle and varied at all time scales, probably due to horizontal advection, local air-sea interaction and vertical mixing. The intermediate layer, between 150 m and 700 m, was characterised by a significant intra-seasonal variability in temperature and salinity, also strongly intercorrelated. This variability was mostly linked to gyre-scale and mesoscale dynamics rather than the surface forcing. Bottom layer was between 700 and 1000 m and had high variability at all timescales in temperature and salinity, strongly influenced by the Mediterranean Outflow Water (MOW) that appeared at these depths. This paper focuses on the top layer because the euphotic depth was always shallower than 100 m at any time and, therefore, the plankton blooms were restricted to in this layer.

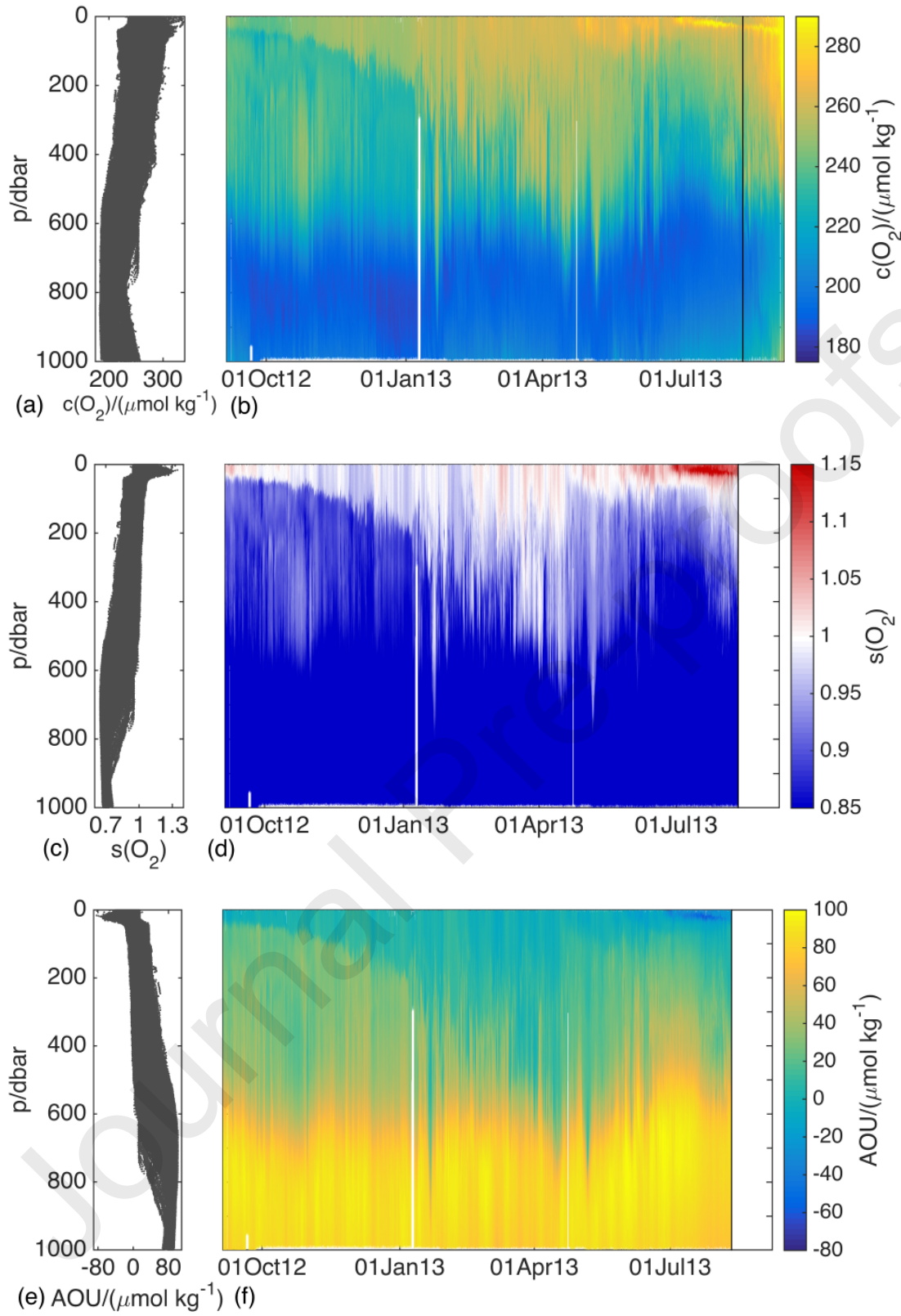


Figure 2 Distribution against pressure (left panel) and time series against pressure (right panel) for (a-b) oxygen concentration, (c-d) oxygen saturation and (e-f) Apparent Oxygen Utilization. The black line in (b) marks the start of the biofouling.

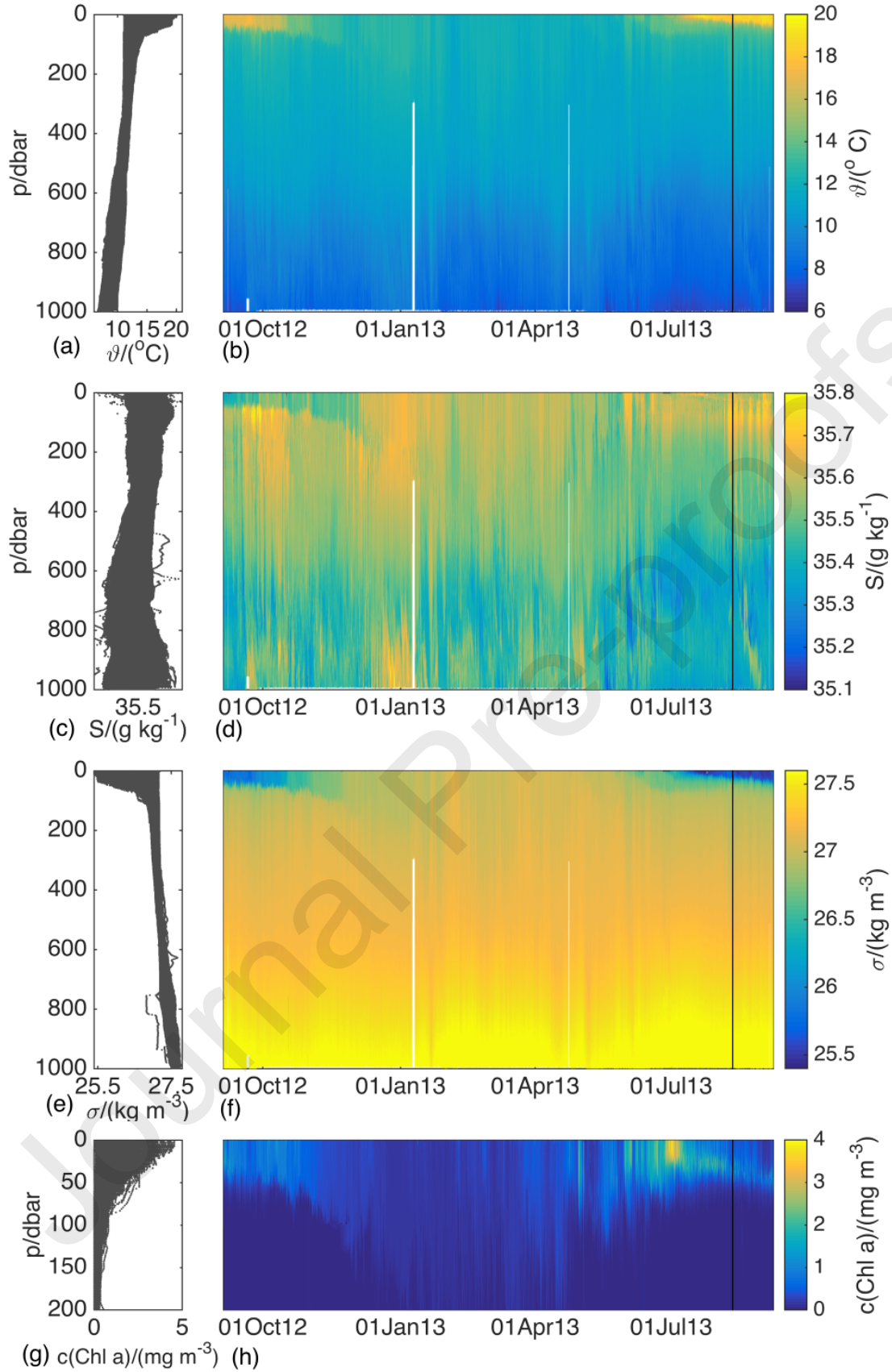


Figure 3 Distribution against pressure (left panel) and time series against pressure (right panel) for (a-b) temperature, (c-d) salinity, (e-f) potential density at surface and (g-h) chlorophyll a concentration above 200 m. The black line in (b-d-f-h) marks the start of the biofouling.

in the top layer,  $c(\text{O}_2)$  varied between  $215 \mu\text{mol kg}^{-1}$  and  $315 \mu\text{mol kg}^{-1}$  and  $c_{\text{sat}}(\text{O}_2)$  between  $224 \mu\text{mol kg}^{-1}$  and  $273 \mu\text{mol kg}^{-1}$ . During winter  $c(\text{O}_2)$  and  $c_{\text{sat}}(\text{O}_2)$  both increased.  $c(\text{O}_2)$  increased from mid-February onwards (Figure 2b), with an alternation between periods of super- and undersaturation, which is reflected in the alternation of red and blue areas near the surface in Figure 2d. At the beginning of July,  $c(\text{O}_2)$  increased at the top 20 m of the water column, but  $c(\text{O}_2)$  quickly decreased at the very surface above 10 m of depth. At the same moment of this surface depletion, a deep chlorophyll and oxygen maximum developed between 20 m and 40 m of depth (Figure 2b and Figure 3h). High  $s(\text{O}_2)$  (up to 1.18) and negative AOU ( $-44 \mu\text{mol kg}^{-1}$ ) were measured in this shallow oxygen maximum (from 14th to 28th July between 10 m and 20 m). The  $s(\text{O}_2)$  and  $c(\text{Chl } a)$  are correlated for  $c(\text{Chl } a)$  higher than  $0.5 \text{ mg m}^{-3}$ . In Figure 4 it is possible to see a tendency to higher  $s(\text{O}_2)$  when there was higher  $c(\text{Chl } a)$  (Figure 4c-d).  $s(\text{O}_2)$  for  $c(\text{Chl } a)$  lower than  $0.5 \text{ mg m}^{-3}$  were influenced by physical rather than biological processes because the algal biomass was too low to produce significant quantities of  $\text{O}_2$ . This was particularly obvious from September to March (Figure 4). Data from July and August showed higher  $s(\text{O}_2)$  with respect to March-June.

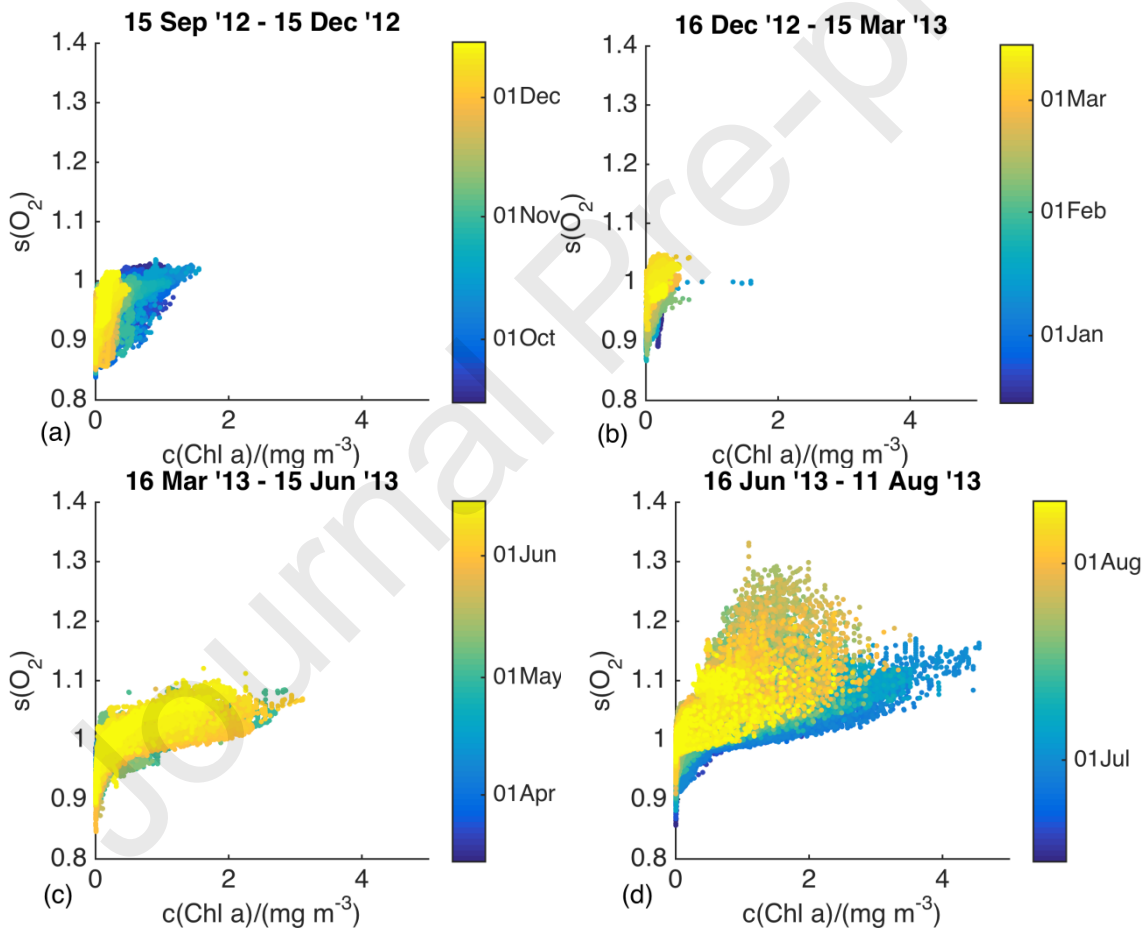


Figure 4 Distribution of oxygen saturation against chlorophyll *a* concentration coloured by the date of measurements between mid-September 2012 and mid-December 2012 (a), mid-December 2012 and mid-March 2013 (b), mid-March 2013 and mid-June 2013 (c) and mid-June 2013 to mid-August 2013 (d).



In order to calculate  $\mathcal{N}$ , the physical factors affecting  $c(\text{O}_2)$  variations ( $F_{\text{as}}$  and  $E$ ) were calculated.  $F_{\text{as}}$  depends on the difference between  $c(\text{O}_2)$  and  $c_{\text{sat}}(\text{O}_2)$  following Eq. 5 (Figure 5a). There was supersaturation ( $c(\text{O}_2) > c_{\text{sat}}(\text{O}_2)$ ) in September at the beginning of the timeseries and after May. There was a period of undersaturation ( $c(\text{O}_2) < c_{\text{sat}}(\text{O}_2)$ ) lasting from November until March and then a period of quasi equilibrium from March to May.  $F_{\text{as}}$  varied between  $-193 \text{ mmol m}^{-2} \text{ d}^{-1}$  and  $155 \text{ mmol m}^{-2} \text{ d}^{-1}$ , with a mean value of  $(-13 \pm 53) \text{ mmol m}^{-2} \text{ d}^{-1}$ .  $F_{\text{as}}$  showed a strong seasonality, with a short period of outgassing at the beginning of the timeseries, followed by a long period of ingassing from the end of September to the beginning of March (Figure 5c). This was in turn followed by two months of quasi equilibrium with weaker influx and, from the end of May,  $F_{\text{as}}$  switched sign and started a period of outgassing that lasted until the end of the mission. Over nearly an annual cycle, this region of the North Atlantic is shown here to be a sink of oxygen rather than a source, with  $4.8 \text{ mol m}^{-2}$  of  $\text{O}_2$  absorbed by the ocean during the surveyed period. This is driven by pulses of strong influx due to high wind that induce high bubble influx ( $\Delta$ , Figure 5b), but also by the late-occurring supersaturation. The data after 11<sup>th</sup> August 2013 were disregarded because of biofouling, making the time series one month shorter than an annual cycle (see Appendix A). This missing month was probably a productive period and therefore its inclusion would have likely increased the magnitude of the annual outgassing if taken into account.

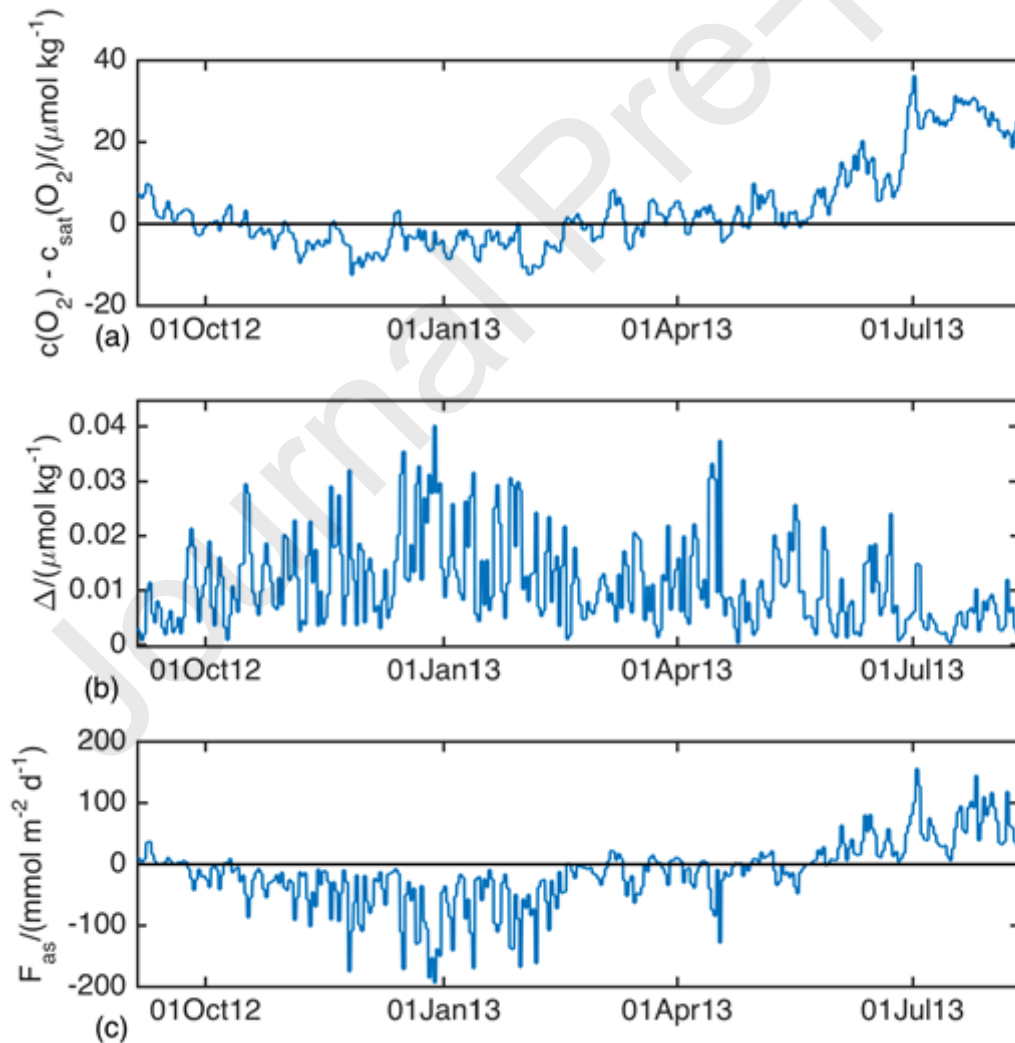




Figure 5 (a) Difference between daily mean oxygen concentration and daily mean oxygen concentration at saturation in the top 10 m used in the air-sea oxygen flux calculation. Positive values indicate supersaturation and negative values indicate undersaturation; (b) bubbles supersaturation parameterisation ( $\Delta$ ) according to Woolf and Thorpe (1991); (c) air-sea oxygen flux. Positive values indicate outgassing of oxygen in the atmosphere and negative values indicate influx of oxygen in the water column.

The other element in the calculation of  $N$  was entrainment,  $E$ . When  $z_{\text{mix}}$  did not deepen below  $z_{\text{lim}}$ ,  $E$  was considered to be zero (Figure 6). When  $z_{\text{mix}}$  deepened, but remained above  $z_{\text{lim}}$ , it was assumed that a redistribution of the  $I(z_{\text{lim}})$  occurred without any  $\text{O}_2$  flux occurring through  $z_{\text{lim}}$ . Also, when  $z_{\text{mix}}$  shoaled, the change in  $I(z_{\text{lim}})$  was assumed not to be related to any mixing with deeper water masses below  $z_{\text{lim}}$  and, therefore, no  $E$  was assumed to occur.

Fluctuation in  $z_{\text{mix}}$  linked to geographical variability and to the sensitivity of the threshold used for  $z_{\text{mix}}$  computation would affect  $E$  because deepening events are not compensated by the shoaling events in the calculation. In order to mitigate the effect of  $z_{\text{mix}}$  variability on  $N$  calculation,  $z_{\text{mix}}$  values were smoothed using a moving average filter over 5 datapoints (black line in Figure 6a).

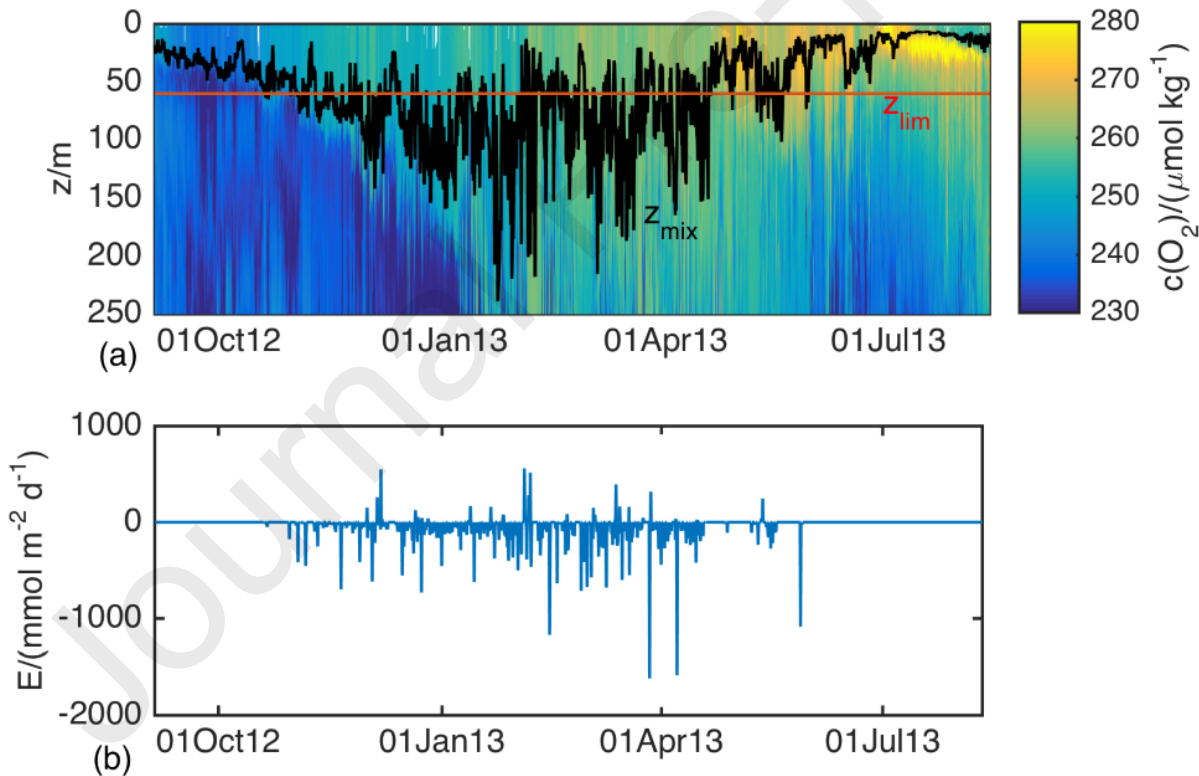


Figure 6 (a) oxygen concentration versus depth with smoothed mixing layer depth (black line) and  $z_{\text{lim}} = 60$  m (red line); (b) entrainment flux, i.e. rate of change of oxygen concentration due to entrainment.

The values of  $N$  were calculated as the variation in  $\alpha(\text{O}_2)$  ( $\Delta I$ ) between consecutive profiles not explainable by  $F_{as}$  and  $E$ . Values were averaged over one week to disregard the effect of advection in the area. The time series of  $N$  averaged in overlapping bins of 7 days is plotted in Figure 7 along with the averaged values of  $\Delta I(z_{lim})/\Delta t$ ,  $F_{as}$  and  $E$ . The cumulative  $N$  between September 2012 and August 2013 is  $6.4 \text{ mol m}^{-2}$  and the mean  $N$  was  $19 \text{ mmol m}^{-2} \text{ d}^{-1}$ . These values show net autotrophy in the area over an annual cycle.

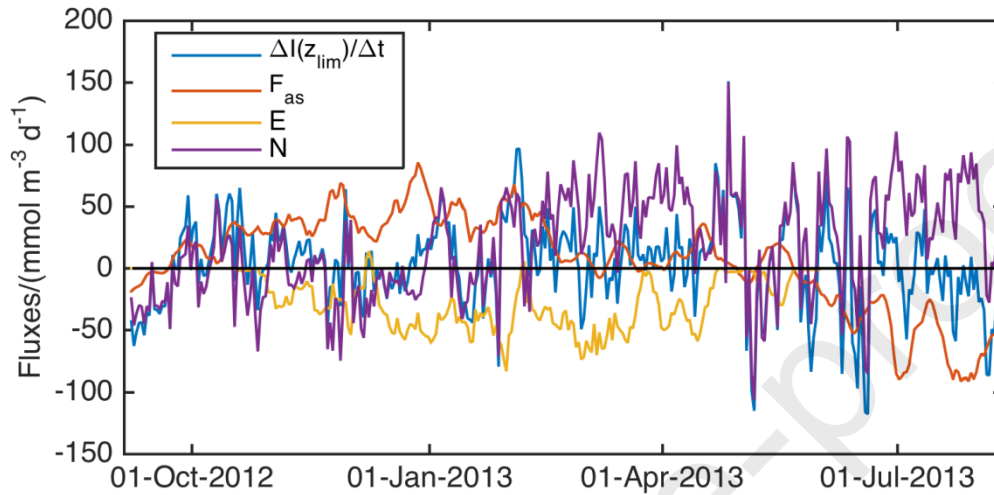


Figure 7 Time series of oxygen fluxes:  $\Delta I(z_{lim})/\Delta t$  in blue,  $F_{as}$  in red,  $E$  in yellow and  $N$  in purple, calculated as in Equation 4. All values are 7-day averages. Note that sign of air-sea  $\text{O}_2$  flux is here inverted in order to represent its contribution to  $N$ .

Four periods (Table 1) were recognized within the cycle of  $N$  (Figure 8). First period is the autumn season between 15<sup>th</sup> September and 20<sup>th</sup> November 2012. From 21<sup>st</sup> November,  $N$  dropped to negative values for several weeks, apart for some positive peaks. Towards the end of this mostly heterotrophic period,  $N$  started oscillating and from 10<sup>th</sup> February remained positive until the 3<sup>rd</sup> May. This long autotrophic period is here considered the start of the spring period. After other oscillations at the end of the spring period, another prolonged period of positive  $N$  starting from 20<sup>th</sup> June is considered as the start of the summer period, with the development of a deep chlorophyll maximum, DCM, and a shallow oxygen maximum.

Table 1 Periods showing different productive regimes identified in the annual cycle with start and end dates and length in days.

| Period               | Start and end date                                     | Length |
|----------------------|--|--------|
| Autumn bloom         | 15 <sup>th</sup> Sep 2012 – 20 <sup>th</sup> Nov 2012  | 67 d   |
| Heterotrophic period | 21 <sup>st</sup> Nov 2012 – 9 <sup>th</sup> Feb 2013   | 81 d   |
| Spring               | 10 <sup>th</sup> Feb 2013 – 19 <sup>th</sup> June 2013 | 130 d  |
| Summer and DCM       | 19 <sup>th</sup> Jun 2013 – 11 <sup>th</sup> Aug 2013  | 54 d   |

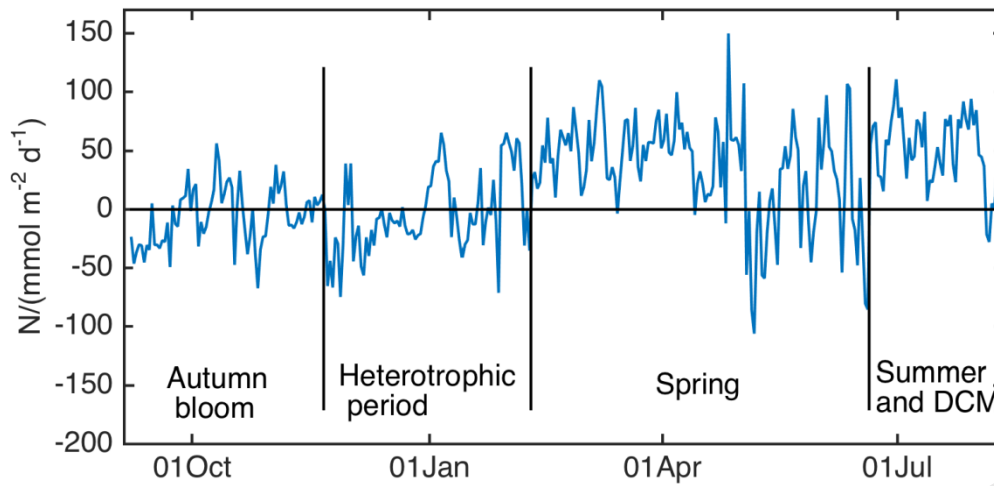


Figure 8 Time series from September 2012 to August 2013 of net community production in oxygen equivalent divided in the four periods analysed separately.

### 3.2 Autumn bloom

During the autumn period, net autotrophy alternated with net heterotrophy (Figure 9a). During the first switch from net respiration to net production on the 27<sup>th</sup> September  $N$  reached a magnitude of  $(16 \pm 12) \text{ mmol m}^{-2} \text{ d}^{-1}$  in oxygen equivalent. This peak in productivity lasted until 2<sup>nd</sup> October, and at the same time chlorophyll  $a$  concentration,  $c(\text{Chl } a)$ , increased as well (Figure 7d) as already discussed by Rumyantseva et al. (2015). They linked this peak to the passage of a storm that was in the area from the 24<sup>th</sup> to the 27<sup>th</sup> September 2012, as shown by the  $U_{10}$  values (Figure 9c).

After 8<sup>th</sup> and 18<sup>th</sup> October,  $N$  and  $c(\text{Chl } a)$  increased again when the wind slowed down after sharp peaks (interpreted as storms). Between 30<sup>th</sup> October and 6<sup>th</sup> November,  $z_{\text{mix}}$  gradually deepened (black line in Figure 9b) and  $N$  peaked again. However, when the wind slowed down and  $z_{\text{mix}}$  shoaled on the 6<sup>th</sup> November,  $N$  had negative values and  $c(\text{Chl } a)$  lowered, showing a decrease in productivity presumably due to a cut-off of nutrient supply from the deep. Afterwards,  $U_{10}$  increased and pushed  $z_{\text{mix}}$  deep again, possibly increasing the amount of nutrients in the water. However,  $z_{\text{mix}}$  did not stabilize again above  $z_{\text{eup}}$ , which could explain the absence of peaks in chlorophyll and the limited productivity.

Despite the production of  $432 \text{ mmol m}^{-2}$  (average  $(17 \pm 14) \text{ mmol m}^{-2} \text{ d}^{-1}$ ) during the autotrophic peaks, the community heterotrophy brings a net balance indistinguishable from 0  $(11 \pm 23) \text{ mmol m}^{-2} \text{ d}^{-1}$  between 26<sup>th</sup> September 2012 and 22<sup>nd</sup> November 2012.

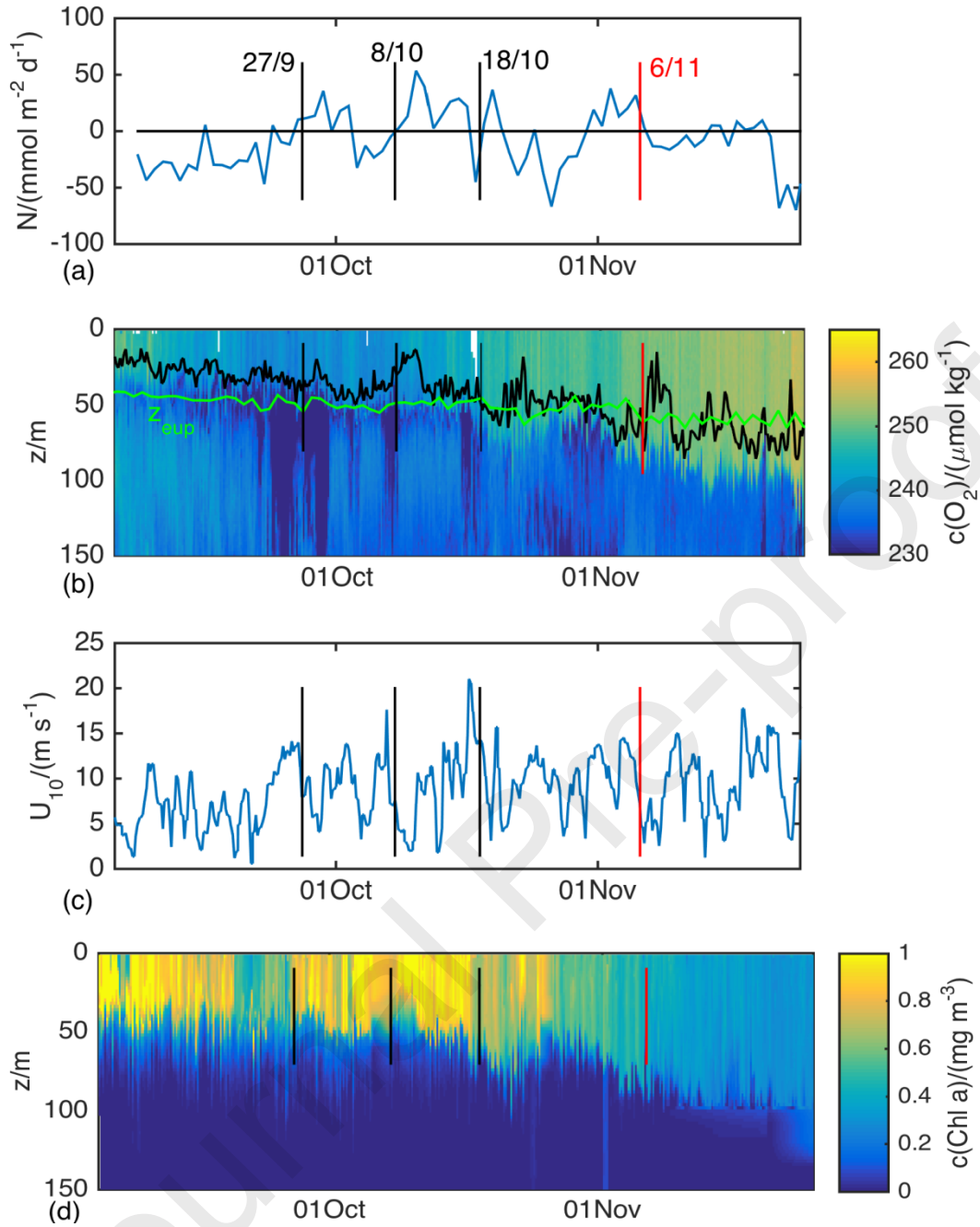


Figure 9 (a) running average of  $N$  over 7 days, (b) mixed layer and euphotic depths over oxygen concentration versus depth, (c) wind speed and (d) chlorophyll a concentration versus depth during the autumn bloom. Black vertical lines indicate the end of wind speed increases (storms) after which there was an increase in biological productivity. Red vertical line marks decrease in wind speed linked to the switch between net autotrophy and net heterotrophy during mixed layer depth shoaling.

### 5.3 Heterotrophic period

The period between 21<sup>st</sup> November 2012 and 9<sup>th</sup> February 2013 was characterised by a long initial period of heterotrophy (Figure 10a;  $N < 0$  for 62 % of the time). Net consumption in the area was calculated at  $-0.3 \text{ mol m}^{-2}$ .

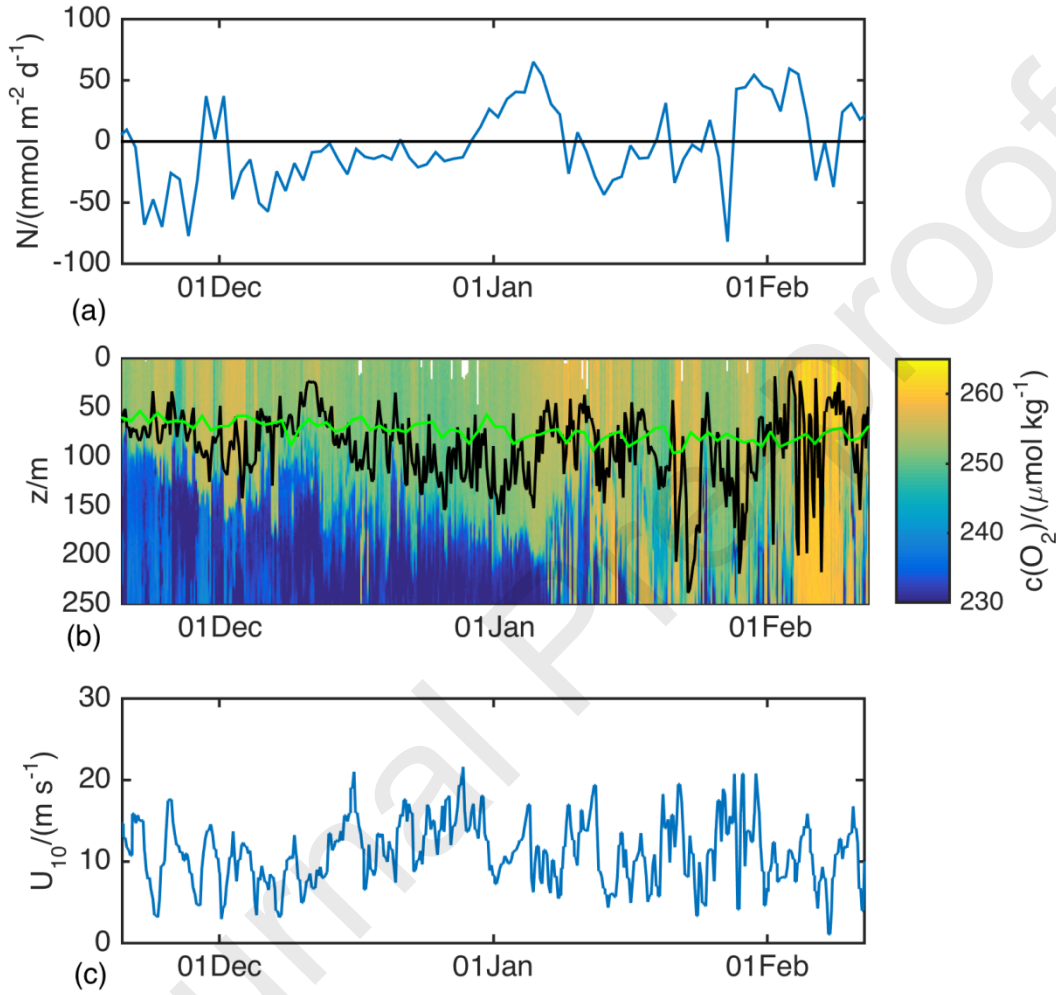


Figure 10 (a) Net community production during the heterotrophic period; (b) oxygen concentration time series versus depth with  $z_{\text{mix}}$  (black line) and euphotic depth (green line); (c) wind speed at 10 m from sea surface from ERA-Interim reanalysis.

Despite the mean  $N$  in this period was  $(-3 \pm 34) \text{ mmol m}^{-2} \text{d}^{-1}$ , the community seemed to go through a train of short peaks in production. These peaks (Figure 11a) coincided with sharp changes in potential density (visible in Figure 11c), and this horizontal heterogeneity suggests that the glider was probably crossing a mesoscale feature, as discussed by Thompson et al. (2016). These are therefore likely false increases in  $N$ , since not related to biological activity. A valid correction for these values was not considered in this study and they were considered in the annual calculation of  $N$ . However, they represent an overestimation of biological  $N$ .

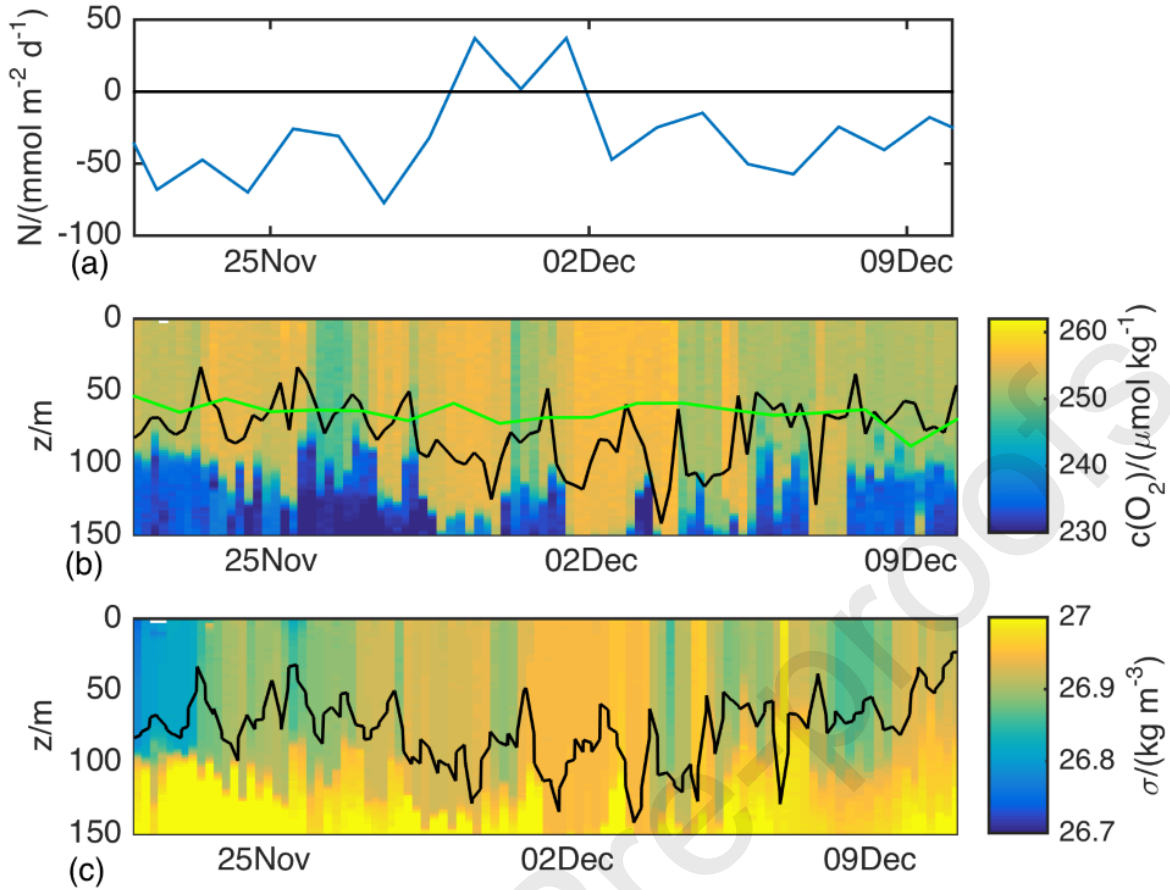


Figure 11 (a)  $N$ , (b) oxygen concentration with euphotic depth in green and mixed layer in black and (c) potential density measured during the spike in  $N$  at the beginning of the heterotrophic period with mixed layer depth based on density. The obvious relation between variations in  $c(O_2)$  and potential density ( $\sigma$ ) suggests the presence of mesoscale features in the area.

Between 30<sup>th</sup> December 2012 and 9<sup>th</sup> January 2013 there was a gradual transition towards a shallower  $z_{mix}$ , which eventually became shallower than  $z_{eup}$  (Figure 10b). This coincided with high  $N$  exceeding 65 mmol m<sup>-2</sup> d<sup>-1</sup>. In the same way, a decrease in wind speed and the shoaling of  $z_{mix}$  to the depth of  $z_{eup}$  coincided with the peak between 28<sup>th</sup> January and 6<sup>th</sup> February.

### 3.4 Spring

The spring season is here defined as the period between 10<sup>th</sup> February 2013 and 19<sup>th</sup> June 2013, 130 days during which the area was autotrophic ( $N > 0$ ) with cumulative  $O_2$  production of 4.5 mol m<sup>-2</sup> and a mean  $N$  of (34±44) mmol m<sup>-2</sup> d<sup>-1</sup> (Figure 11). In this period, however, there was high variability ( $N$  standard deviation = 44 mmol m<sup>-2</sup> d<sup>-1</sup>) because production alternated with net respiration from the beginning of May (Figure 13). Six 7-day bins of  $N$  estimates were above 100 mmol m<sup>-2</sup> d<sup>-1</sup> with a maximum of 149 mmol m<sup>-2</sup> d<sup>-1</sup>.

The period showed a series of  $N$  fluctuations. In February, despite minimal variations in  $c(Chl\ a)$ ,  $N$  is high. High levels of  $U_{10}$  are linked to periodic deepening of  $z_{mix}$ , that is however usually above  $z_{eup}$ , which indicate



an increase in the amount of light experienced by the cells and, therefore, a boost in productivity. This also coincide with a period of  $H$  oscillating between negative and positive values, after a period of strong negative values. Another obvious feature is a short chlorophyll bloom happening in the upper 50 m of the water column between 24<sup>th</sup> and 28<sup>th</sup> February 2013, here called ‘End-February Event’ (EFE, Figure 12a). This event happened when  $z_{\text{mix}}$  was very shallow (20-25 m), wind decreased and net heat flux ( $H$ , Figure 12e) became temporarily positive (heat from the atmosphere to the ocean).

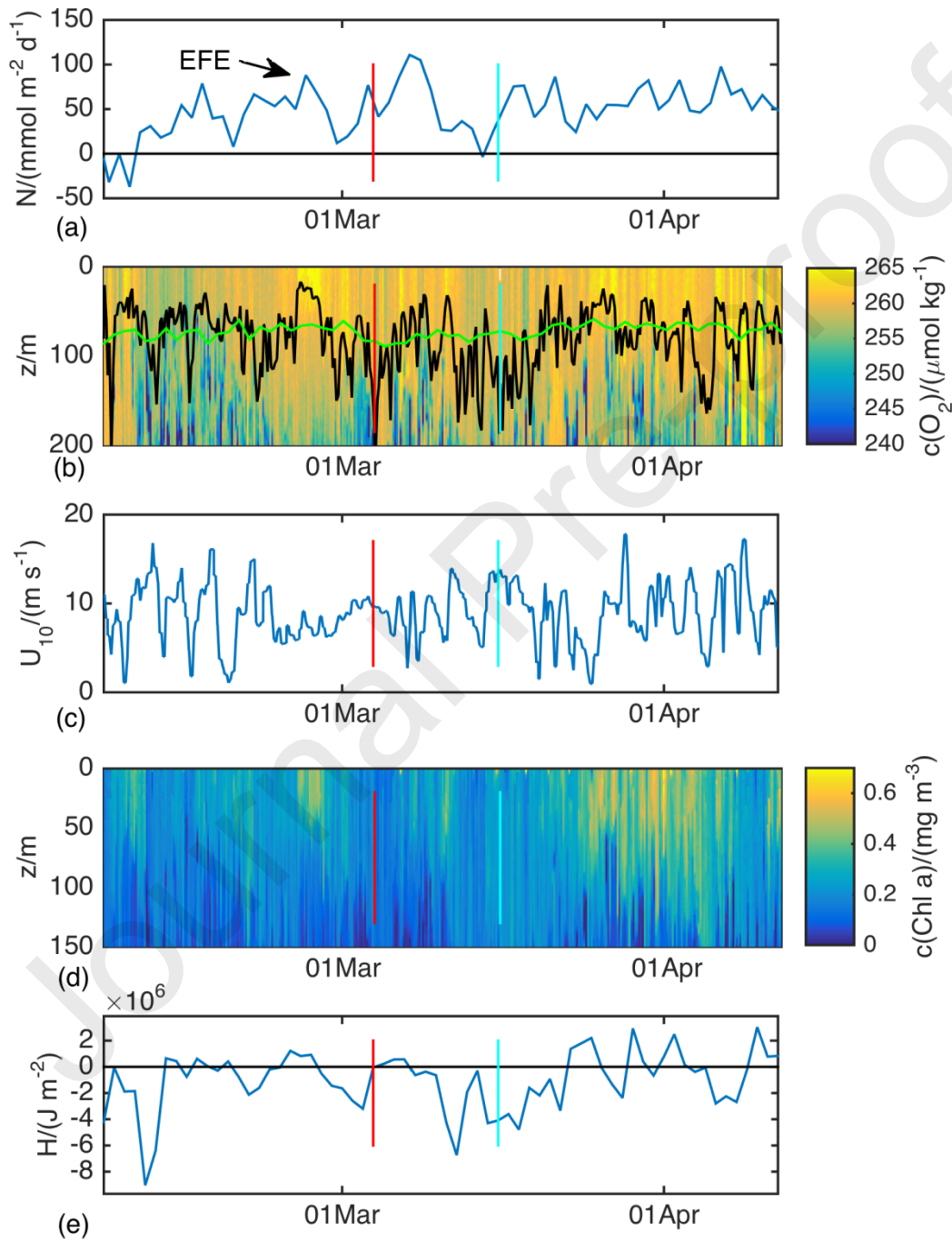


Figure 12 (a)  $N$ , (b) mixed layer (black line) and euphotic depths (green line) over oxygen concentration versus depth, (c) wind speed, (d) chlorophyll a concentration versus depth and (e) net heat flux between (positive, heat from atmosphere to the ocean) 9th February

and 12th April. Black vertical line indicates the start of the peak on 4<sup>th</sup> March and light blue line the start of the peak on 10<sup>th</sup> March. In panel (a) one can also see the peak associated with the end-February event (EFE).

A larger peak in  $N$  occurred between 4th and 10th March when wind slowed down,  $H$  became temporarily positive again and  $z_{\text{mix}}$  shoaled with respect to  $z_{\text{eup}}$ . Another peak was visible between 16<sup>th</sup> March and 11<sup>th</sup> April 2013 when  $z_{\text{mix}}$  started to shoal again showing a reduction in mixing and, arguably, in turbulence.  $H$  was still negative, but it gradually increased towards a period of more stable positive values. During this peak  $z_{\text{mix}}$  varied significantly and  $N$  showed small decreases in its magnitude every time  $z_{\text{mix}}$  deepened and peaks every time  $z_{\text{mix}}$  shoaled near the surface.

The main spring bloom happened between 19<sup>th</sup> April and 27<sup>th</sup> May (Figure 13), showing a substantial increase in  $c(\text{Chl } a)$ .  $z_{\text{mix}}$  shoaled and stayed mostly stable above  $z_{\text{eup}}$ . This happened 10 days later than the switch of the heat flux from being mostly negative (water cooling) to mostly positive (water warming). However,  $N$  increased only when wind speed decreased on 19<sup>th</sup> April. The water retained at the surface became warmer and lighter, accumulating phytoplankton biomass. However, after 15 days (3<sup>rd</sup> May),  $N$  decreased suddenly, followed by a decrease in  $c(\text{Chl } a)$ . Another interesting event starts on the 16<sup>th</sup> May, when wind speed increased and  $z_{\text{mix}}$  deepened. There was a slight increase of potential density and slight decrease of temperature showing that water from below the  $z_{\text{eup}}$ , probably enriched in nutrients, was mixed to the surface. Wind then decreased and  $N$  increased for a brief time, followed by an increase in  $c(\text{O}_2)$  below  $z_{\text{mix}}$  rather than above, which could be evidence of low nutrient concentrations at the surface.

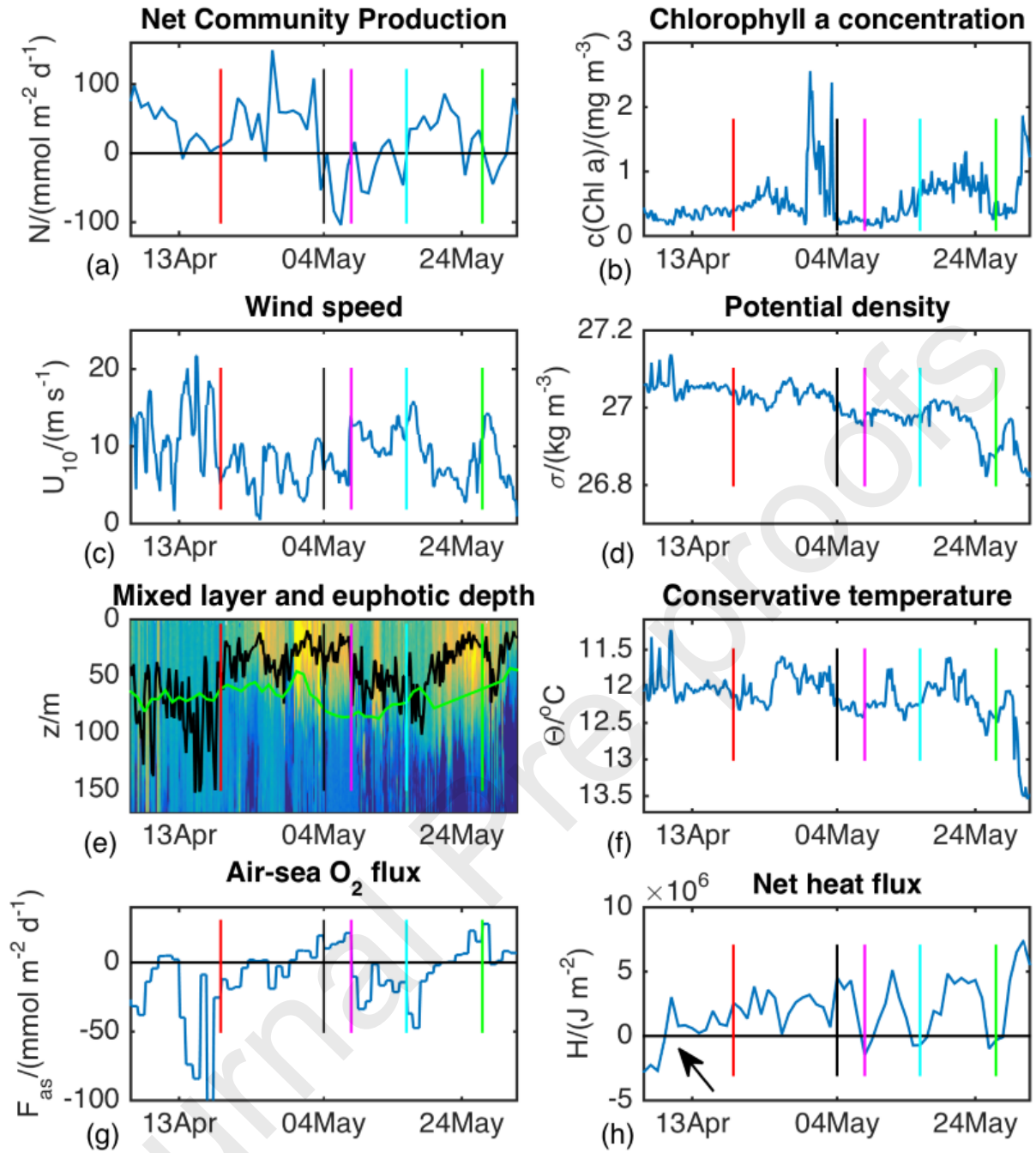


Figure 13 Parameters associated with the  $N$  peak between April 19<sup>th</sup> and May 27<sup>th</sup>. (a) net community production above 60 m, (b) mean chlorophyll a concentration above 60 m, (c) wind speed (Era-Interim reanalysis), (d) mean potential density in the top 10 m, (e) mixed layer depth (in blue) and euphotic depth (in red) with background colours showing oxygen variations., (f) mean temperature in the top 10 m, (g) air-sea flux including bubbles and (h) net heat flux (ERA-Interim reanalysis). Red vertical line is the beginning of the peak (April 19<sup>th</sup>), black vertical line is the beginning of the heterotrophic period (May 4<sup>th</sup>), pink vertical line is the end of it (May 8<sup>th</sup>), light blue vertical line is the deepening event replenishing the nutrients above  $z_{mix}$  (May 16<sup>th</sup>) and green line is the end of the productive peak (May 27<sup>th</sup>).

### 3.5 Summer bloom and deep chlorophyll maximum

From 20<sup>th</sup> June onwards,  $N$  was relatively high and above zero and  $z_{mix}$  was always shallower than  $z_{eup}$  (Figure 14). This summer period as a whole had a mean  $N$  of  $(47 \pm 36)$  mmol m<sup>-2</sup> d<sup>-1</sup> and produced 2.5 mol m<sup>-2</sup>. The main features in this period are a surface bloom between 26<sup>th</sup> June and 4<sup>th</sup> July and the development of a deep

chlorophyll maximum (DCM). The surface bloom was very productive with a mean  $N$  of  $(71 \pm 24)$  mmol m<sup>-2</sup> d<sup>-1</sup>, reaching 110 mmol m<sup>-2</sup> d<sup>-1</sup>. However, since it lasted only 8 days, it produced only 0.6 mol m<sup>-2</sup>. There was also an increase in  $c(\text{Chl } a)$ . The bloom ended when wind increased again and  $z_{\text{mix}}$  deepened.

From 8<sup>th</sup> July wind decreased (Figure 14c) and the water column transitioned to a regime of low turbulence and strong stratification. A DCM developed and the production increased significantly. Both the subsurface oxygen- and chlorophyll-rich feature were above the  $z_{\text{eup}}$  of 60 m. During the time in which there was a DCM, the system remained productive until 4<sup>th</sup> August, when the productivity decreased along with an increase in wind speed, potentially leading to increased turbulence in the water.  $z_{\text{mix}}$  deepened within the DCM, eroding it and mixing it with surface waters. The decrease of  $N$  at the end of the DCM period occurred at the same time as a decrease in the  $c(\text{Chl } a)$ . During the presence of DCM (30 days, 8<sup>th</sup> July to 8<sup>th</sup> August) 1.5 mol m<sup>-2</sup> were produced with a mean  $N$  of  $(48 \pm 32)$  mmol m<sup>-2</sup> d<sup>-1</sup>.

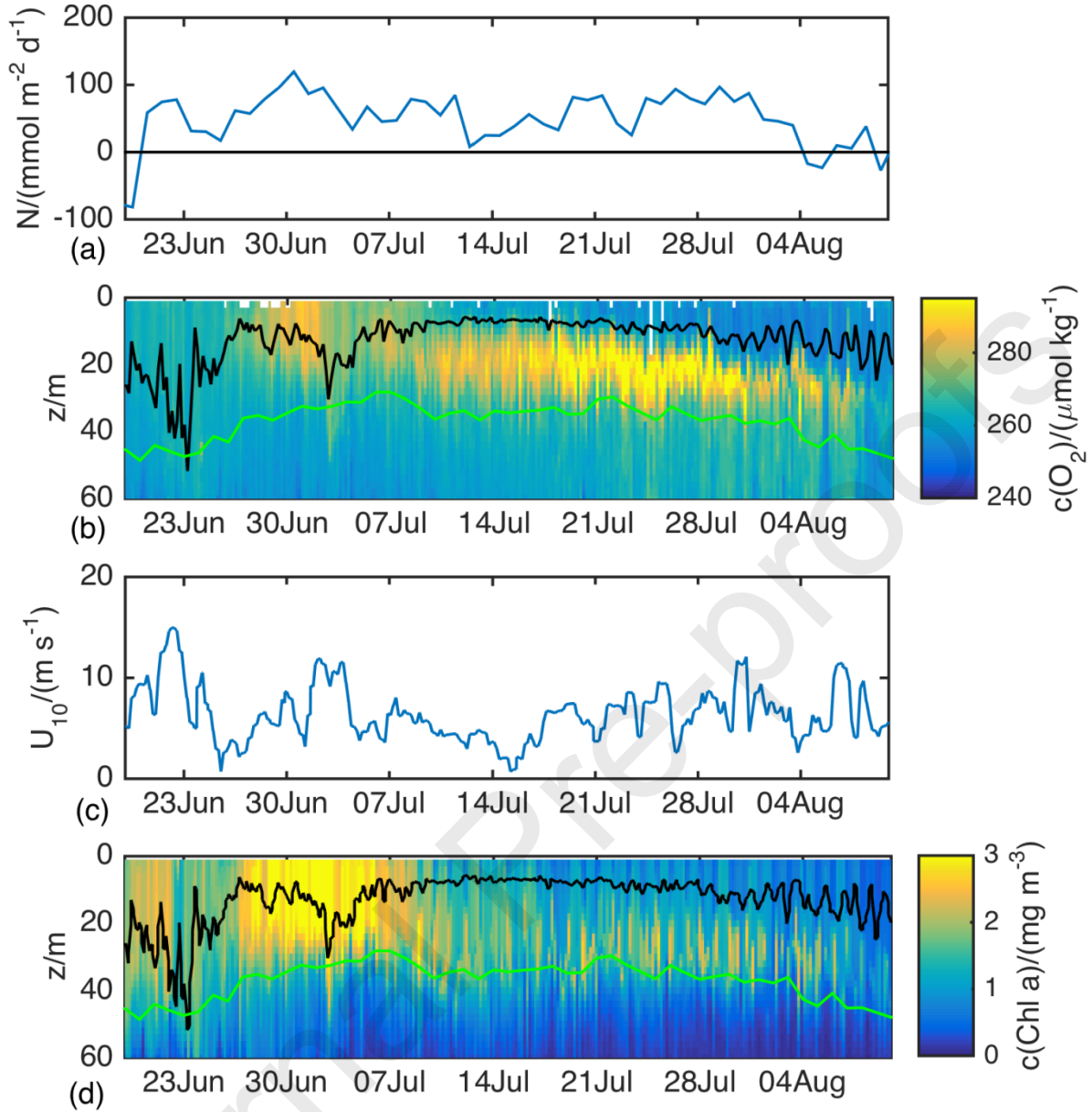


Figure 14 (a) Net community production during the summer bloom and the deep chlorophyll maximum; (b) oxygen concentration over depth and time above  $z_{lim}$  with  $z_{mix}$  (black line) and  $z_{eup}$  (green line); (c) wind speed at 10 m above sea-surface from ERA-Interim reanalysis; (d) chlorophyll a concentration versus depth.

## 4 Discussion

### 4.1 Annual cycle of $N$

This study calculated the productivity of the plankton community at the Porcupine Abyssal Plain for an annual cycle based on variations in  $c(O_2)$ . Data were acquired between surface and 1000 m depth, but the analysis focused on the production in the euphotic layer, which was always within the upper  $\sim 100$  m of the water

column. In winter, colder temperatures increased  $c_{\text{sat}}(\text{O}_2)$  and triggered an influx of  $\text{O}_2$  from the atmosphere that, considering the absence of substantial biological activity and the rapid gas exchange due to strong winds, was expected to equilibrate to saturation (Broecker and Peng, 1992; Woolf and Thorpe, 1991; Chester, 2000; Ito et al., 2004). However, the water stayed undersaturated during this period showing that the air-sea  $\text{O}_2$  flux was not sufficient to saturate the water. These results confirm previous observations (e.g. Körtzinger et al., 2001; Russell and Dickson, 2003; Körtzinger et al., 2004; Keeling et al., 2010; Duteil et al., 2013) and model output (Ito et al., 2004), which also reported undersaturation in surface waters in several oceans.

Supersaturation was expected in the upper ocean during phytoplankton blooms, when biological production peaks. Biological processes increased  $c(\text{O}_2)$  from mid-February onwards, but supersaturation was not persistent. The level of  $c_{\text{sat}}(\text{O}_2)$  suggests that, instead of a continuous bloom, a series of minor blooms occurred from February onwards before the major spring bloom that started at the end of May, when  $c(\text{Chl } a)$  increased significantly. Assuming that air-sea flux works towards saturating water over time, then oxygen production by phytoplankton in an already saturated water mass should result in supersaturation ( $s(\text{O}_2) > 0$ ). However, considering that the air-sea flux was not sufficient to equilibrate  $s(\text{O}_2)$ , it can also be argued that increases in  $c(\text{O}_2)$  due to biological production might not always be enough for  $s(\text{O}_2) > 0$ . For this reason, the analysis of the production should not be based only on the supersaturation pattern and potential increases of  $c(\text{Chl } a)$  in periods of undersaturation should be investigated analysing variations in oxygen budget.

At the end of the main bloom (beginning of July),  $c(\text{O}_2)$  decreased at the surface, while a deep chlorophyll and oxygen maximum developed between 10 m and 20 m from 14th to 28th July. The level of  $s(\text{O}_2)$  in relation to  $c(\text{Chl } a)$  seems to change between spring and summer, when  $s(\text{O}_2)$  reaches the highest value of 1.18. This different relation could be related to a change in the phytoplankton community between spring and summer: the community of the deep chlorophyll maximum seems able more efficient, being able to produce more  $\text{O}_2$  and supersaturate the water at lower  $c(\text{Chl } a)$  with respect to earlier periods of the year. Changes in the phytoplankton community, such as the succession of dominant species over time, are linked to variation in parameters in the water column; the decrease of silicates after the uptake during diatom blooms, is one of the phenomena that can drive these successions (Egge and Aksnes, 1992; Martin-ezequel et al, 2000) making diatoms bloom before autotrophic dinoflagellates (Margalef, 1978; Leterme et al., 2005; McQuatters-Gollop et al., 2007, Barton et al., 2013). Furthermore, dimensional classes within the same group show a succession related to the ability of smaller species to uptake nutrients more efficiently in oligotrophic environments (Barton et al., 2013). This might also be related to the cyclic changes in nitrate concentration shown in the area by Hartman et al. (2010). The changes in the length of day light has also been linked to changes in bacterioplankton composition, which in turn has been linked to changes in phytoplankton (Gilbert et al., 2012). Considering that each taxon produces a different amount of oxygen per mole of chlorophyll a, a change in the dominant taxa when productivity is moved in the deep chlorophyll maximum could explain the higher amount of oxygen per unit chlorophyll. It must also be considered that the same species have variations in its amount of chlorophyll a, for example because of photoacclimation (Sakshaug et al. 1997; Goericke and Montoya 1998; Henriksen et al. 2002), which means that variations in the amount of chlorophyll a per cell do not change



linearly with the amount of  $O_2$  produced. This shift in species and/or in the physiology of the cems is influenced by many environmental factors such as light intensity, nutrient availability or the regime of turbulence (e.g., Huisman et al., 2004; Veldhuis et Kraay, 2004; Brunet et al., 2008; Dimier et al., 2009, Barton et al., 2013). Considering that the formation of the summer deep chlorophyll maximum suggests a substantial attenuation of mixing forces and that the end of the main bloom can be related to low nutrients, it is reasonable to induce that environmental changes drove a shift in the phytoplankton community, which led to higher saturation per unit chlorophyll in the DCM. It shall be also considered that the reduced turbulence might have given time to phytoplankton to adapt to different levels of light and that photosensitivity might therefore have played a game in reducing productivity at the top of the water column.

The productive period (spring and summer together) spanned from 9<sup>th</sup> February to the start of biofouling on 11<sup>th</sup> August and had a time-integrated oxygen production of  $(7.1 \pm 2.1)$  mol  $m^{-2}$  with a mean  $N$  of  $(39 \pm 41)$  mmol  $m^{-2} d^{-1}$ . The seasonal production was converted to C equivalents using the photosynthetic quotient (PQ) of 1.5 as in Alkire et al., (2014) and resultant  $N_C$  values are listed in Table 3.

Considering only the productive period, our study region produced  $N_C = (4.8 \pm 1.4)$  mol  $m^{-2}$ . This value is lower than the  $(6.4 \pm 1.1)$  mol  $m^{-2}$  estimated by Körtzinger et al. (2008a) but fits well with the  $(4.6 \pm 0.9)$  mol  $m^{-2}$  estimated by Frigstad et al. (2015) for the PAP area over a similar time span.  $N_C$  is higher than the 3.0 mol  $m^{-2}$  estimated by Ostle et al. (2015) on a basin scale and the 2.1 mol  $m^{-2}$  estimated by Alkire et al. (2014) in a more northerly area (59 °N instead of 49 °N). The results therefore suggest that the region of the PAP site is particularly productive. In these comparisons it must be considered that previous studies focused on shorter productive periods, leaving unresolved the question on whether the ocean over one year is either a heterotrophic or an autotrophic system. The current results show autotrophy over the entire annual cycle in the productive top layer despite long period of heterotrophy (see section 4.3). This result fits with previous works that show net production when incubation-free methods are used (Letscher and Moore, 2017) and support the position that this part of the ocean has positive net production. Despite the major focus of discussion about the trophic state of the ocean has been focused mostly on subtropical oligotrophic gyres (e.g., Williams et al., 2013; Duarte et al, 2013), our results should be taken in account in global budgeting to estimate the carbon cycle and to consider whether the ocean is a net sink or source of carbon.

Considering the whole time series, the PAP site was autotrophic between September 2012 and August 2013, with annually integrated net community  $O_2$  production of  $(6.4 \pm 1.9)$  mol  $m^{-2} a^{-1}$  ( $(4.3 \pm 1.3)$  mol  $m^{-2}$  in C equivalents). This value was computed without the last month of the year, which was disregarded due to biofouling on the optode. However, the shape of the biofouled profiles showed a DCM above 60 m (data not shown). Biofouling and its progressive growth also show a productive phytoplankton community. The disregarded period can therefore be considered productive and the cumulative  $N$  of 6.4 mol  $m^{-2}$  is likely an underestimation of the real production in the area over the full year.

The annual production values are higher than previous annual  $N_C$  estimates of Quay et al. (2012) who estimated 2.8 mol  $m^{-2}$  in the subpolar North Atlantic Ocean or by Neuer et al. (2007) who estimated  $N_C = 3.3$  mol  $m^{-2}$  as

a mean between 1996 and 2000 in a more southerly area. The annual production estimated in the present study is instead similar to the  $5.5 \text{ mol m}^{-2}$  estimated by Ostle et al. (2015) for 2012 in their region 2 (where PAP site is located). This area was found in their study to be the most productive sector in the basin. This similarity, however, hide seasonal differences since estimates from Ostle et al. (2015) are lower during the productive period and higher during the winter.

The differences among studies are probably due to factors such as interannual variability in the area and differences in methods used for the calculations.  $N$  in the present study was an estimate of the production in the euphotic layer and, therefore, studies analysing variation at greater depths than  $z_{\text{eup}}$  are expected to be lower because of the respiration occurring deeper. For example, some of the studies compared here (e.g., Frigstad et al., 2015; Ostle et al., 2015) analyse the changes above  $z_{\text{mix}}$  rather than above  $z_{\text{eup}}$ , while others (i.e. Körtzinger et al., 2008a) use deeper  $z_{\text{lim}}$  (230 m) for the calculation of  $I(\text{O}_2)$ . The temporal patchiness of productivity also increases the variability among  $N$  estimates, especially when values are averaged over subsamples in the same productive period (Alkire et al., 2012).

*Table 2 Net community production in carbon equivalent,  $N_C$  (adapted and expanded from Alkire et al. 2014). In bold are the results from studies analysing  $N_C$  directly, while in normal characters are the estimates in oxygen unit converted to  $N_C$  using the photosynthetic quotient, PQ. In these cases the PQ value used for the conversion is indicated.*

| Study                                   | Year        | Period   | $N_C$<br>$\text{mmol m}^{-2} \text{ d}^{-1}$ | PQ<br>used | Notes  |
|---|-------------|--|--|------------|--|
| This study                              | 2013        | Autumn Bloom<br>Spring<br>19 Apr – 3 May<br>Summer<br>26 Jun – 4 Jul<br>DCM<br>Spring+Summer<br>Whole year | 11<br>22<br>54<br>31<br>46<br>32<br>26<br>13 | 1.5        | PAP station,<br>top<br>60 m                      |
| <b>Bender et al.,<br/>1992</b>          | <b>1989</b> | <b>13 days<br/>between<br/>Apr and May</b>   | <b>52</b>                                    |            | <b>JGOFS,<br/>North<br/>Atlantic<br/>47N/20W</b> |
| <b>Körtzinger et<br/>al.,<br/>2008a</b> | <b>2004</b> | <b>May –Aug</b>  | <b>25</b>                                    |            | <b>PAP station</b>                               |
| <b>Körtzinger et<br/>al.,</b>           | <b>2005</b> | <b>mid May -Jul</b>  | <b>50-70</b>                                 |            | <b>Labrador<br/>Sea</b>                          |

|                                      |                       |                         |                   |     |   |
|--------------------------------------|-----------------------|-------------------------|-------------------|-----|---|
| <b>2008D</b>                         |                       |                         |                   |     |   |
| Alkire et al.<br>2012                | 2008                  | Apr<br>May<br>(average) | 66<br>115<br>(90) | 1.5 | Early Bloom<br>Main Bloom<br>Iceland Basin                          |
| Alkire et al.<br>2014                | 2008                  | Apr-Jun<br>3-26 Jun     | 25<br>43          | 1.5 | Considering<br>Alkire et al.<br>2012<br>+postbloom<br>Iceland Basin |
| Ostle et al.,<br>2015                | 2012                  | Apr - Sep               | 16                | 0.8 | Basin-wide,<br>region 2 (see<br>Ostle et al.,<br>2015)              |
| <b>Frigstad et<br/>al.,<br/>2015</b> | <b>2003-<br/>2012</b> | <b>Feb - July 25</b>    | <b>(72-6)</b>     |     | <b>PAP site,<br/>Mixed Layer</b>                                    |

#### 4.2 Bloom initiation dynamics

Measuring  $N$  based on oxygen variations (direct by-product of photosynthesis) shows that heterotrophy and autotrophy alternate throughout the whole year. Different processes seem to trigger autotrophic peaks at different times of year. During autumn (nutrient limitation),  $N$  peaks have been related to pulses of nutrients created by the interaction between wind and surface currents (see Rumyantseva et al., 2015). However, the trigger for later  $N$  peaks seems to follow instead the gradual deepening of the mixed layer into nutrient-rich waters, a dynamic already suggested in previous papers (Marra et al., 1990; Findlay et al., 2006). This process also explains how peaks of  $N$  can develop at the end of the spring, when nutrient can be depleted as well after a big bloom.

When nutrient limitation could be excluded,  $N$  increased only when the mixed layer was shoaling while there was net heterotrophy during the winter, when the mixed layer was deepening. Our results therefore disagree with the Recoupling-Dilution Hypothesis. Instead, the present study presents evidence supporting the validity of the mechanism proposed by Enriquez and Taylor (2015). When nutrients are not limiting, the peaks in  $N$  are associated with decreasing wind speed and positive net heat flux, which in turn are linked to a shoaling mixing layer. Our results imply that the plankton community needs low turbulence conditions in order to bloom. The magnitude of the blooms also seems to be related to the relative depth of the mixing layer to the euphotic depth, rather than the critical depth used in Enriquez and Taylor (2015). The main blooms developed when  $z_{\text{mix}}$  shoaled near or just above  $z_{\text{eup}}$ . The increase of production when the mixing layer shoaled did not always correspond to significant increases of chlorophyll  $a$  concentration at the surface (Rumyantseva et al., 2019) but rather subsurface (e.g., the peak starting on 3<sup>rd</sup> March).

Most of the peaks of  $N$  are associated with positive net surface heat flux i.e. ocean warming. In particular, the start of the main bloom during spring coincided with the switch between a period of mean negative net heat flux and a period of mean positive net heat flux at the beginning of April consistent with the HFH theory of Taylor and Ferrari (2011). This suggests that the time of this switch in the sign of net surface heat flux could be used as a proxy to analyse interannual variability in the starting time of the main bloom. However,  $N$  increased after a delay due to the presence of a storm, showing the need to take into consideration the turbulence induced by the wind stress in order to have more accurate bloom timing estimates, as hypothesised by Chiswell (2011) and Brody et al. (2013).

This study also highlights the presence of peaks in productivity when chlorophyll concentration showed no variations, which have to be considered along with the chlorophyll fluorescence-defined blooms in order to analyse correctly the triggering factors that increase production. It is also important to use high temporal resolution *in situ* data instead of climatologies to better appreciate the high variability of the system. The use of the mixing layer depth instead of the mixed layer depth is important to analyse variations in turbulence that affect the plankton and its metabolic activity.

### 4.3 Autumn period

The presence of increased productivity during the autumn is well known for this part of the ocean and is usually referred as the “autumn bloom” (Colebrook, 1982; Longhurst, 1995; Dandonneau et al., 2004; Lévy et al., 2005; Neuer et al., 2007; Martinez et al., 2011). The term ‘bloom’ however suggests a prolonged period of stable productivity, which was not observed in this data series. In the present study in fact, a series of autotrophic peaks happened in this season at the end of storms. Production enhancement after storms has already been seen in previous studies (Babin et al., 2004; Son et al., 2006; Wu et al., 2008; Rummyantseva et al., 2015). This supports the notion that autumn blooms are sustained by nutrient pulses through the pycnocline due to shear spiking (Rippeth et al., 2005; Rippeth et al., 2009; Williams et al., 2013; Rummyantseva et al., 2015) generated by rapid change in wind stress (Pollard, 1980). This suggests that pulses of nutrients from below stimulate biological production in shallow and nutrient depleted mixed layers. In these post-storm blooms, wind has to decrease before  $N$  could peak.

In contrast, the last peak of this season (30<sup>th</sup> October to 6<sup>th</sup> November) was linked to the gradual deepening of  $z_{\text{mix}}$  and the introduction to the surface layer of nutrients from below. The decrease of  $c(\text{Chl } a)$  at the end of this productivity peak (figure 3d) marks the passage to a less productive regime, with  $N$  not increasing even when  $z_{\text{mix}}$  shoaled. This peak seemed therefore to follow the dynamics described by Marra et al. (1990) and Findlay et al. (2006) according to which the nutrient input fuelling the autumn bloom is caused by the gradual deepening of  $z_{\text{mix}}$ . These two different dynamics of  $N$  peaks were discussed by Dutkiewicz et al. (2001), who showed that increasing wind speed can enhance  $N$  by bringing nutrients towards the surface as well as decrease  $N$  moving phytoplankton cells deeper, where they consume more than they produce (for example during storms).

The peaks of productivity during autumn were of lower magnitude than in spring and the total  $N$  was not significantly different from 0. This is in line with the conclusions of Martinez et al. (2011) who showed an asymmetry in the magnitude of the blooms in different seasons. According to Martinez et al. (2011), there was a shift from the 1980s, when autumn blooms had a magnitude comparable with the spring blooms, to the present day, when autumn blooms are smaller than spring blooms, as we find here. Martinez et al. (2011) linked this change to the delayed deepening of  $z_{\text{mix}}$  at the end of the summer that now happens later in the year than in the past.

Lateral advection, presence of mesoscale events, change in zooplankton community or even the effect of wind and storms are other possible causes for the smaller magnitude of autumn blooms proposed by Martinez et al. (2011). The present study supports the conclusions of Martinez et al. (2011) of non-symmetric blooms between seasons, and uses *in situ* measurements to support their hypothesis, which was based on satellite data.

#### 4.4 Heterotrophic period

Heterotrophic periods have been already recorded in the North Atlantic (see literature in Duarte et al., 2013), however their magnitude and impact on the annual metabolic balance are debated (Duarte et al., 2013). Multiannual studies show the inter-annual variability in the metabolic state of the ocean at this time of the year (November-February). Ostle et al. (2015) used basin-scale observations of  $c(\text{O}_2)$  at the surface to measure  $N$  and found autotrophy throughout 2012 and low  $N$  (not statistically different from zero) in 2013.

In this study, pulses of positive  $N$  during the heterotrophic period were linked to the glider crossing a mesoscale feature. The averaging process was probably not able to fully eliminate the signal of this geographical heterogeneity in  $N$  because the feature stayed in the area longer than one week.

The feature crossed by the glider at the end of November – beginning of December 2013 (Figure 11) had higher  $c(\text{O}_2)$  and part of this might be actually due to production. However, the density of the water was lower and an increase in  $c(\text{O}_2)$  was explainable by the solubility effect (higher  $c_{\text{sat}}(\text{O}_2)$ ). This peak was therefore probably overestimating  $N$ .

Other peaks occurred when  $z_{\text{mix}}$  stopped deepening and shoaled above  $z_{\text{eup}}$ . The potential reduction in turbulence in these cases seems to be linked to higher productivity since the  $N$  peaks were interrupted when the wind speed increased again.

The consumption estimated in the heterotrophic period ( $0.3 \text{ mol m}^{-2}$ ) was one order of magnitude lower than the production estimates in the rest of the year. The present study therefore shows that the presence of potentially protracted periods of net heterotrophy in this part of the North Atlantic have only a moderate impact on the production on an annual scale.

#### 4.5 Spring

The PAP site is located in the North Atlantic between the subpolar and subtropical gyres, where, according to Longhurst (1998), blooms are expected in May. The timing of this bloom and its intensity have high interannual

and geographical variability (Ueyama and Monger, 2005; Henson et al., 2006; Henson et al., 2009; Kanru et al., 2011; Zhai et al., 2013; Cole et al., 2015) and this explains why, despite being one of the most studied systems in oceanography, the dynamics of the North Atlantic spring bloom have not been fully understood as yet.

The pattern of several parameters (wind speed,  $z_{\text{mix}}$  in relation to  $z_{\text{eup}}$ , temperature, density, net heat flux) was compared with variations of  $N$ , with several peaks in productivity observed before the main bloom between April and May. Following this comparison, possible explanations for the variations of production over time were suggested: the water near-surface was considered nutrient repleted at the beginning of spring, while nutrient-limitation was assumed to happen later on in the season, considering the seasonal pattern showed by Hartman et al. (2010) in this area. Variations in nutrients availability to phytoplankton could therefore be the cause of the oscillations between  $N > 0$  and  $N < 0$  in the second part of the spring, with phytoplankton becoming more productive when nutrients were supplied. However, the absence of direct measurements of nutrient concentrations in this study makes it difficult to confirm these speculations and extrapolate them to infer more general dynamics. At the end of this period there were rapid transitions between accumulation of oxygen at the surface and below  $z_{\text{mix}}$ . These were probably related to geographical patchiness and demonstrate the heterogeneity of biological production at this time of the year.

#### 4.6 Summer and deep chlorophyll maximum

Changes in nutrient concentrations may have caused the variations of  $N$  seen during the summer. Particularly interesting in this period is the DCM that lasted for over 30 days in the area thanks to a well-stratified water column with a very shallow  $z_{\text{mix}}$  above 10 m. The presence of this feature suggests nutrient limitation in the upper water column, as shown in previous studies (Klausmeier and Litchman, 2001; Klausmeier et al., 2007; Denaro et al., 2013). When the DCM was present,  $N$  integrated stayed high, accounting for 38 % of the cumulative  $N$  estimated throughout the whole study. The formation of the DCM is usually related to increases in biomass (Beckmann and Hense, 2007) and/or to adaptation in the chlorophyll content of the cells (Fennel and Boss, 2003). This feature is a challenge for  $N$  calculations based on remote measurements or on the sampling of the plankton community for *in vitro* incubation. The ocean colour measured by satellite-borne sensors can be biased if the DCM is shallower than  $\sim 45$  m depth study (Stramska and Stramski, 2005), as found in the present, *de facto* decoupling fluorescence readings from the real value at the surface. Annual  $N$  estimates obtained with the method used here should therefore be of higher accuracy and reliability than the ones based on remotely sensed ocean colour.

The demise of the DCM is probably related to nutrient limitation.  $N$  decreased when  $z_{\text{mix}}$  started to deepen at the end of July; however,  $z_{\text{mix}}$  was still above  $z_{\text{eup}}$  and so the reduced productivity was not related to the limitation of light. Instead, wind speed increased and the ensuing vertical turbulence may have exposed the plankton to the nutrient depleted water above, lowering the production. Evidence of this is the decrease of  $c(\text{Chl } a)$  happening at the same time between 20 and 40 m. An alternative explanation could be the reduction



of the photosynthetic performances in the cells due to changes in photosensitivity. The low turbulence could in fact narrow the difference between phytoplankton adaptation time and water mixing time, resulting in changes in the pigment physiology of the cells (Claustre et al., 1994).

From the end of June,  $F_{as}$  was coupled to  $N$  values. The entrainment in this period was negligible, thanks to the strong stratification that allowed the formation of the DCM. This  $F_{as}$  can then be considered biologically induced, as found by Kaiser et al. (2005) for systems with negligible vertical and horizontal mixing.

## 5 Conclusions

Net community production ( $N$ ) above the mean euphotic depth near the PAP site from September 2012 to August 2013 has been calculated by analysing the variations in depth integrated oxygen concentration over time. The area is autotrophic, with a mean  $N$  value of  $19 \text{ mmol m}^{-2} \text{ d}^{-1}$  and a total production of  $6.5 \text{ mol m}^{-2}$  and an estimated annual production of  $7 \text{ mol m}^{-2}$ . The analysis of the annual cycle of net community production shows the presence of four periods with different regimes: the autumn period, a heterotrophic period and two productive periods (spring and summer) separated by the depletion of nutrients after the spring bloom. During the summer a very productive deep chlorophyll maximum developed which was responsible for a significant portion of the annual production. The values calculated fit the range of published estimates of net community production in the North Atlantic basin and in the same area. The variations within this range are attributed in part to the differences among the methods used for the calculations and also to interannual variability.

Variations in production are associated with factors such as wind speed, net heat flux and mixing layer depth. The theories proposed in the last decades for the explanation of the blooms (Critical Depth Hypothesis, Critical Turbulence Hypothesis, Heat-flux Hypothesis) are consistent with each other in explaining different mechanisms for how the system passes from net heterotrophy to net autotrophy when favourable conditions are matched.

## 6. Acknowledgments

This work would not have been possible without the piloting skills of several colleagues at the University of East Anglia, National Oceanography Centre (Southampton) and California Institute of Technology, plus the contribution of many people not represented in the author list. The deployment and recovery operations of gliders has also been possible thanks to the scientists, technicians, officers and crews of the RRS Discovery (cruise D381), RV Celtic Explorer (cruise CE13001), and RRS James Cook (cruises JC085, JC087 and JC090). The study is part of the project OSMOSIS, funded by NERC grants NE/I020083/1 and NE/I019905/1 and supported by NSF award OCE 1155676. UB was supported by Cefas funding during the writing of this paper. GMD and KJH were supported during the writing of this paper by the

European Research Council under the European Union's Horizon 2020 research and innovation programme (grant agreement n° 741120).

ALKIRE, M. B., D'ASARO, E., LEE, C., JANE PERRY, M., GRAY, A., CETINIĆ, I., BRIGGS, N., REHM, E., KALLIN, E., KAISER, J. & GONZÁLEZ-POSADA, A. 2012. Estimates of net community production and export using high-resolution, Lagrangian measurements of O<sub>2</sub>, NO<sub>3</sub><sup>-</sup>, and POC through the evolution of a spring diatom bloom in the North Atlantic. *Deep Sea Research Part I: Oceanographic Research Papers*, 64, 157-174.

ALKIRE, M. B., LEE, C., D'ASARO, E., PERRY, M. J., BRIGGS, N., CETINIĆ, I. & GRAY, A. 2014. Net community production and export from Seaglider measurements in the North Atlantic after the spring bloom. *Journal of Geophysical Research: Oceans*, 119, 6121-6139.

BABIN, S. M., CARTON, J. A., DICKEY, T. D. & WIGGERT, J. D. 2004. Satellite evidence of hurricane-induced phytoplankton blooms in an oceanic desert. *Journal of Geophysical Research: Oceans*, 109.

BARTON, A.D., FINKEL, Z.V., WARD, B.A., JOHNS, D.G., FOLLOWS, M.J., 2013. On the roles of cell size and trophic strategy in North Atlantic diatom and dinoflagellate communities, *Limnology and Oceanography*, 58, DOI: 10.4319/lo.2013.58.1.0254.

BECKMANN, A. & HENSE, I. 2007. Beneath the surface: Characteristics of oceanic ecosystems under weak mixing conditions – A theoretical investigation. *Progress in Oceanography*, 75, 771-796.

BEHRENFELD, M. J. 2010. Abandoning Sverdrup's Critical Depth Hypothesis on phytoplankton blooms. *Ecology*, 91, 977-989.

BENDER, M., DUCKLOW, H. W., KIDDON, J., J., M. & MARTIN, J. 1992. The carbon balance during the 1989 spring bloom in the North Atlantic Ocean, 47N/20W. *Deep Sea Research*, 39, 1707-1725.

BENSON, B.B. AND KRAUSE, D., 1984. The concentration and isotopic fractionation of oxygen dissolved in freshwater and seawater in equilibrium with the atmosphere<sup>1</sup>. *Limnology and oceanography*, 29(3), pp.620-632.

BRODY, S.R., LOZIER, M.S. and DUNNE, J.P. 2013. A comparison of methods to determine phytoplankton bloom initiation. *Journal of Geophysical Research: Oceans*, 118(5), pp.2345-2357.

BROECKER, W. S. & PENG, T.-H. 1992. Interhemispheric transport of carbon dioxide by ocean circulation. *Nature*, 356, 587-589.

BRUNET, C., CASOTTI, R. & VANTREPOTTE, V. 2008. Phytoplankton diel and vertical variability in photobiological responses at a coastal station in the Mediterranean Sea. *Journal of Plankton Research*, 30, 645-654.

CASTRO-MORALES, K. & KAISER, J. 2012. Using dissolved oxygen concentrations to determine mixed layer depths in the Bellingshausen Sea. *Ocean Science*, 8, 1-10.

CHISWELL, S.M., 2011. Annual cycles and spring blooms in phytoplankton: don't abandon Sverdrup completely. *Marine ecology progress series*, 443, pp.39-50. COLE, H. S., HENSON, S., MARTIN, A. P. & YOOL, A. 2015. Basin-wide mechanisms for spring bloom initiation: how typical is the North Atlantic? ICES Journal of Marine Science: Journal du Conseil.

CLAUSTRE, H., KERHERVÉ, P., MARTY, J.C. & PRIEUR, L., 1994. Phytoplankton photoadaptation related to some frontal physical processes. *Journal of Marine Systems*, 5(3-5), pp.251-265.

COLEBROOK, J. M. 1982. Continuous plankton records: seasonal variations in the distribution and abundance of plankton in the North Atlantic Ocean and the North Sea. *Journal of Plankton Research*, 4, 435-462.

CULBERSON, C. H. 1991. Dissolved Oxygen. WHP Operations and Methods. Unpublished manuscript,, 15pp.

DAMERELL, G. M., HEYWOOD, K. J., THOMPSON, A. F., BINETTI, U. & KAISER, J. 2016. The Vertical Structure of Upper Ocean Variability at the Porcupine Abyssal Plain during 2012-2013. *J. Geophys. Res. - Oceans*, Submitted.

DANDONNEAU, Y., DESCHAMPS, P.-Y., NICOLAS, J.-M., LOISEL, H., BLANCHOT, J., MONTEL, Y., THIEULEUX, F. & BÉCU, G. 2004. Seasonal and interannual variability of ocean color and composition of phytoplankton communities in the North Atlantic, equatorial Pacific and South Pacific. *Deep Sea Research Part II: Topical Studies in Oceanography*, 51, 303-318.

DE BOYER MONTEGUT, C., MADEC, G., FISCHER, A. S., LAZAR, A. & IUDICONE, D. 2004. Mixed layer depth over the global ocean: An examination of profile data and a profilebased climatology. *J. Geophys. Res.*, 109.

DEL GIORGIO, P. A., COLE, J. J. & CIMBLERIS, A. 1997. Respiration rates in bacteria exceed phytoplankton production in unproductive aquatic systems. *Nature*, 385, 148-151.

DEL GIORGIO, P. A. & DUARTE, C. M. 2002. Respiration in the open ocean. *Nature*, 420, 379-384.

DENARO, G., VALENTI, D., LA COGNATA, A., SPAGNOLO, B., BONANNO, A., BASILONE, G., MAZZOLA, S., ZGOZI, S. W., ARONICA, S. & BRUNET, C. 2013. Spatiotemporal behaviour of the deep chlorophyll maximum in Mediterranean Sea: Development of a stochastic model for picophytoplankton dynamics. *Ecological Complexity*, 13, 21-34.

DICKSON, A. G. 1996. Determination of dissolved oxygen in seawater by Winkler titration. WOCE Operations Manual. Volume 3: The Observational Programme. Volume 3. Section 3.1: WOCE Hydrographic Programme. Part 3.1.3: WHP Operations and Methods, edited by World Ocean Circulation Experiment, Woods Hole, Massachusetts, USA.

DIMIER, C., GIOVANNI, S., FERDINANDO, T. & BRUNET, C. 2009. Comparative Ecophysiology of the Xanthophyll Cycle in Six Marine Phytoplanktonic Species. *Protist*, 160, 397-411.

DUARTE, C. M. & AGUSTÍ, S. 1998. The CO<sub>2</sub> Balance of Unproductive Aquatic Ecosystems. *Science*, 281, 234-236.

- DUARTE, C. M., REGAUDIE-DE-GIOUX, A., ARRIETA, J. M., DELGADO-HUERTAS, A. & AGUIAR, S. 2013. The Oligotrophic Ocean Is Heterotrophic. *Annual Review of Marine Science*, 5, 551-569.
- DUCKLOW, H. W. & DONEY, S. C. 2013. What is the metabolic state of the oligotrophic ocean? A debate. *Annual review of marine science*, 5, 525-533.
- DUTEIL, O., KOEVE, W., OSCHLIES, A., BIANCHI, D., GALBRAITH, E., KRIEST, I. & MATEAR, R. 2013. A novel estimate of ocean oxygen utilisation points to a reduced rate of respiration in the ocean interior. *Biogeosciences*, 10, 7723-7738.
- DUTKIEWICZ, S., FOLLOWS, M., MARSHALL, J. & GREGG, W. W. 2001. Interannual variability of phytoplankton abundances in the North Atlantic. *Deep Sea Research Part II: Topical Studies in Oceanography*, 48, 2323-2344.
- EGGE, J.K. & AKSNES, D.L., 1992. Silicate as regulating nutrient in phytoplankton competition. *Marine ecology progress series*. Oldendorf, 83(2), pp.281-289.
- EMERSON, S., STUMP, C. & NICHOLSON, D. 2008. Net biological oxygen production in the ocean: Remote in situ measurements of O<sub>2</sub> and N<sub>2</sub> in surface waters. *Global Biogeochemical Cycles*, 22, GB3023.
- ENRIQUEZ, R. M. & TAYLOR, J. R. 2015. Numerical simulations of the competition between wind-driven mixing and surface heating in triggering spring phytoplankton blooms. *ICES Journal of Marine Science: Journal du Conseil*, 72, 1926-1941.
- FALKOWSKI, P. G., BARBER, R. T. & SMETACEK, V. 1998. Biogeochemical Controls and Feedbacks on Ocean Primary Production. *Science*, 281, 200-206.
- FENNEL, K. & BOSS, E. 2003. Subsurface maxima of phytoplankton and chlorophyll: Steadystate solutions from a simple model. *Limnology and Oceanography*, 48, 1521-1534.
- FIELD, C. B., BEHRENFELD, M. J., RANDERSON, J. T. & FALKOWSKI, P. 1998. Primary Production of the Biosphere: Integrating Terrestrial and Oceanic Components. *Science*, 281, 237-240.
- FINDLAY, H. S., YOOL, A., NODALE, M. & PITCHFORD, J. W. 2006. Modelling of autumn plankton bloom dynamics. *Journal of Plankton Research*, 28, 209-220.
- FRANKS, P. J. 2014. Has Sverdrup's critical depth hypothesis been tested? Mixed layers vs. turbulent layers. *ICES J. Mar. Sci.*, 1-11.
- FRIGSTAD, H., HENSON, S. A., HARTMAN, S. E., OMAR, A. M., JEANSSON, E., COLE, H., PEBODY, C. & LAMPITT, R. S. 2015. Links between surface productivity and deep ocean particle flux at the Porcupine Abyssal Plain sustained observatory. *Biogeosciences*, 12, 5885-5897.
- GARCIA, H. E. & GORDON, L. I. 1992. Oxygen solubility in seawater: better fitting equations. *Limnology & Oceanography*, 37, 1307-1312.
- GILBERT, J.A., STEELE, J.A., CAPORASO, J.G., STEINBRÜCK, L., REEDER, J., TEMPERTON, B., HUSE, S., MCHARDY, A.C., KNIGHT, R., JOINT, I. & SOMERFIELD, P., 2012. Defining seasonal marine microbial community dynamics. *The ISME journal*, 6(2), p.298.

- GOERCKE, R., MONTÓYA, J.P., 1998. Estimating the contribution of microalgal taxa to chlorophyll *a* in the field variations of pigment ratios under nutrient and light-limited growth. *Mar Ecol Prog Ser* 169:97–112
- HAMME, R. C. & EMERSON, S. 2006. Constraining bubble dynamics and mixing with dissolved gases: Implications for productivity measurements by oxygen mass balance. *Journal of Marine Research*, 64, 73-95.
- HANSELL, D. A., CARLSON, C. A., REPETA, D. J. & SCHLITZER, R. 2009. Dissolved organic matter in the ocean: A controversy stimulates new insights. *Oceanography*, 22, 202-211.
- HARTMAN, S.E., LARKIN, K.E., LAMPITT, R.S., LANKHORST, M. & HYDES, D.J., 2010. Seasonal and inter-annual biogeochemical variations in the Porcupine Abyssal Plain 2003–2005 associated with winter mixing and surface circulation. *Deep Sea Research Part II: Topical Studies in Oceanography*, 57(15), pp.1303-1312.
- HENSON, S. A., DUNNE, J. P. & SARMIENTO, J. L. 2009. Decadal variability in North Atlantic phytoplankton blooms. *Journal of Geophysical Research: Oceans* (1978–2012), 114.
- HENRIKSEN, P., RIEMANN, B., KAAS, H., SØRENSEN, H.M., SØRENSEN, H.L., 2002. Effects of nutrient-limitation and irradiance on marine phytoplankton pigments. *J Plankton Res* 24:835–858
- HENSON, S. A., ROBINSON, I., ALLEN, J. T. & WANIEK, J. J. 2006. Effect of meteorological conditions on interannual variability in timing and magnitude of the spring bloom in the Irminger Basin, North Atlantic. *Deep Sea Research Part I: Oceanographic Research Papers*, 53, 1601-1615.
- HUISMAN, J., OOSTVEEN, P. V. & WEISSING, F. J. 1999. Critical Depth and Critical Turbulence: Two Different Mechanisms for the Development of Phytoplankton Blooms. *Limnology and Oceanography*, 44, 1781-1787.
- HUISMAN, J., SHARPLES, J., STROOM, J. M., VISSER, P. M., KARDINAAL, W. E. A., VERSPAGEN, J. M. H. & SOMMEIJER, B. 2004. Changes in turbulent mixing shift competition for light between phytoplankton species. *Ecology*, 85, 2960-2970.
- HULL, T., GREENWOOD, N., KAISER, J. & JOHNSON, M. 2016. Uncertainty and sensitivity in optode-based shelf-sea net community production estimates. *Biogeosciences*, 13, 934-959.
- ITO, T., FOLLOWS, M. J. & BOYLE, E. A. 2004. Is AOU a good measure of respiration in the oceans? *Geophysical Research Letters*, 31, n/a-n/a.
- KAHRU, M., BROTHAS, V., MANZANO-SARABIA, M. & MITCHELL, B. G. 2011. Are phytoplankton blooms occurring earlier in the Arctic? *Global Change Biology*, 17, 1733-1739.
- KAISER, J., REUER, M. K., BARNETT, B. & BENDER, M. L. 2005. Marine productivity estimates from continuous O<sub>2</sub>/Ar ratio measurements by membrane inlet mass spectrometry. *Geophysical research letters*, 32.
- KARL, D. M., LAWS, E. A., MORRIS, P., WILLIAMS, P. J. L. & EMERSON, S. 2003. Global carbon cycle (communication arising): Metabolic balance of the open sea. *Nature*, 426, 32-32.
- KEELING, R. F., KÖRTZINGER, A. & GRUBER, N. 2009. Ocean Deoxygenation in a Warming World. *Annual Review of Marine Science*, 2, 199-229.

- KLAUSMEIER, C. A. & LITCHMAN, E. 2001. Algal games: The vertical distribution of phytoplankton in poorly mixed water columns. *Limnology & Oceanography*, 46, 1998-2007.
- KLAUSMEIER, C. A., LITCHMAN, E. & LEVIN, S. A. 2007. A model of flexible uptake of two essential resources. *Journal of Theoretical Biology*, 246, 278-289.
- KÖRTZINGER, A., KOEVE, W., KÄHLER, P. & MINTROP, L. 2001. C:N ratios in the mixed layer during the productive season in the northeast Atlantic Ocean. *Deep Sea Research Part I: Oceanographic Research Papers*, 48, 661-688.
- KÖRTZINGER, A., SCHIMANSKI, J., SEND, U. & WALLACE, D. 2004. The Ocean Takes a Deep Breath. *Science*, 306, 1337-1337.
- KÖRTZINGER, A., SEND, U., LAMPITT, R. S., HARTMAN, S., WALLACE, D. W. R., KARSTENSEN, J., VILLAGARCIA, M. G., LLINÁS, O. & DEGRANDPRE, M. D. 2008a. The seasonal pCO<sub>2</sub> cycle at 49°N/16.5°W in the Northeastern Atlantic Ocean and what it tells us about biological productivity. *Journal of Geophysical Research: Oceans*, 113, C04020.
- LETERME, S. C., M. EDWARDS, L. SEURONT, M. J. ATTRILL, P. C. REID, AND A. W. G. JOHN. 2005. Decadal basin-scale changes in diatom, dinoflagellates, and phytoplankton color across the North Atlantic. *Limnol. Oceanogr.* 50: 1244–1253, DOI:10.4319/lo.2005.50.4.1244.
- LÉVY, M., LEHAHN, Y., ANDRÉ, J.-M., MÉMERY, L., LOISEL, H. & HEIFETZ, E. 2005. Production regimes in the northeast Atlantic: A study based on Sea-viewing Wide Field-of-view Sensor (SeaWiFS) chlorophyll and ocean general circulation model mixed layer depth. *Journal of Geophysical Research: Oceans*, 110.
- MARGALEF, R., 1978. Life-forms of phytoplankton as survival alternatives in an unstable environment. *Oceanol. Acta* 1: 493–509.
- MARRA J., BIDIGARE, R. R. & D., D. T. 1990. Nutrients and mixing, chlorophyll and phytoplankton growth. *Deep Sea Research* 37, 127-143.
- MARTINEZ, E., ANTOINE, D., D'ORTENZIO, F. & DE BOYER MONTÉGUT, C. 2011. Phytoplankton spring and fall blooms in the North Atlantic in the 1980s and 2000s. *Journal of Geophysical Research: Oceans*, 116.
- MCQUATTERS-GOLLOP, A., D. RAITOS, M. EDWARDS, AND M. J. ATTRILL. 2007. Spatial patterns of diatom and dinoflagellate seasonal cycles in the NE Atlantic Ocean. *Mar. Ecol. Prog. Ser.* 339: 301–306, DOI:10.3354/meps339301
- NEUER, S., CIANCA, A., HELMKE, P., FREUDENTHAL, T., DAVENPORT, R., MEGGERS, H., KNOLL, M., SANTANA-CASIANO, J. M., GONZÁLEZ-DAVILA, M., RUEDA, M.-J. & LLINÁS, O. 2007. Biogeochemistry and hydrography in the eastern subtropical North Atlantic gyre. Results from the European time-series station ESTOC. *Progress in Oceanography*, 72, 1-29.
- NICHOLSON, D., EMERSON, S. & ERIKSEN, C. C. 2008. Net community production in the deep euphotic zone of the subtropical North Pacific gyre from glider surveys. *Limnology and Oceanography*, 53, 2226-2236.



- NICHOLSON, D. P., WILSON, S. T., DONEY, S. C. & KARL, D. M. 2015. Quantifying subtropical North Pacific gyre mixed layer primary productivity from Seaglider observations of diel oxygen cycles. *Geophys. Res. Lett.*, 42, 4032-4039.
- OSTLE, C., JOHNSON, M., LANDSCHÜTZER, P., SCHUSTER, U., HARTMAN, S., HULL, T. & ROBINSON, C. 2015. Net community production in the North Atlantic Ocean derived from Volunteer Observing Ship data. *Global Biogeochemical Cycles*, 29, 80-95.
- POLLARD, R. T. 1980. Properties of Near-Surface Inertial Oscillations. *Journal of Physical Oceanography*, 10, 385-398.
- QUAY, P. D., STUTSMAN, J. & STEINHOFF, T. 2012. Primary production and carbon export rates across the subpolar N. Atlantic Ocean basin based on triple oxygen isotope and dissolved O<sub>2</sub> and Ar gas measurements. *Global Biogeochemical Cycles*, 26.
- REGAUDIE-DE-GIOUX, A., LASTERNAS, S., AGUSTÍ, S. & DUARTE, C. 2014. Comparing marine primary production estimates through different methods and development of conversion equations. *Frontiers in Marine Science*, 1.
- RIPPETH, T. P., PALMER, M. R., SIMPSON, J. H., FISHER, N. R. & SHARPLES, J. 2005. Thermocline mixing in summer stratified continental shelf seas. *Geophysical Research Letters*, 32.
- RIPPETH, T. P., WILES, P., PALMER, M. R., SHARPLES, J. & TWEDDLE, J. 2009. The diapycnal nutrient flux and shear-induced diapycnal mixing in the seasonally stratified western Irish Sea. *Continental Shelf Research*, 29, 1580-1587.
- RUMYANTSEVA, A., LUCAS, N., RIPPETH, T., MARTIN, A., PAINTER, S. C., BOYD, T. J. & HENSON, S. 2015. Ocean nutrient pathways associated with the passage of a storm. *Global Biogeochemical Cycles*, 29, 1179-1189.
- RUMYANTSEVA, A., A., HENSON, S., MARTIN, A., THOMPSON, A.F., DAMERELL, G. M., KAISER, K., HEYWOOD, K. J. 2019. Phytoplankton spring bloom initiation: The impact of atmospheric forcing and light in the temperate North Atlantic Ocean. Submitted to the same special issue.
- RUSSELL, J. L. & DICKSON, A. G. 2003. Variability in oxygen and nutrients in South Pacific Antarctic Intermediate Water. *Global Biogeochemical Cycles*, 17.
- SAKSHAUG, E., BRICAUD, A., DANDONNEAU, Y., FALKOWSKI, P.G., KIEFER, D.A., LEGENDRE, L., MOREL, A., PARSLOW, J. & TAKAHASHI, M., 1997. Parameters of photosynthesis: definitions, theory and interpretation of results. *Journal of Plankton Research*, 19(11), pp.1637-1670.
- SON, S., PLATT, T., BOUMAN, H., LEE, D. & SATHYENDRANATH, S. 2006. Satellite observation of chlorophyll and nutrients increase induced by Typhoon Megi in the Japan/East Sea. *Geophysical Research Letters*, 33.
- STRAMSKA, M. and STRAMSKI, D., 2005. Effects of a nonuniform vertical profile of chlorophyll concentration on remote-sensing reflectance of the ocean. *Applied Optics*, 44(9), pp.1735-1747.
- SVERDRUP, H. U. 1953. On Conditions for the Vernal Blooming of Phytoplankton. *Journal du Conseil*, 18, 287-295.

- TAYLOR, J. R. & FERRARI, R. 2011. Shutdown of turbulent convection as a new criterion for the onset of spring phytoplankton blooms. *Limnology and Oceanography*, 56, 2293-2307.
- TENGBERG, A., HOVDENES, J., ANDERSSON, H., BROCANDEL, O., DIAZ, R., HEBERT, D., ARNERICH, T., HUBER, C., KÖRTZINGER, A., KHRIPOUNOFF, A., REY, F., RONNING, C., SCHIMANSKI, J., SOMMER, S. & STANGELMAYER, A. 2006. Evaluation of a lifetime-based optode to measure oxygen in aquatic systems. *Limnol. Oceanogr. Methods*, 4, 7-17.
- UEYAMA, R. & MONGER, B. C. 2005. Wind-induced modulation of seasonal phytoplankton blooms in the North Atlantic derived from satellite observations. *Limnology and Oceanography*, 50, 1820-1829.
- VELDHUIS, M. J. W. & KRAAY, G. W. 2004. Phytoplankton in the subtropical Atlantic Ocean: towards a better assessment of biomass and composition. *Deep Sea Research Part I: Oceanographic Research Papers*, 51, 507-530.
- WILLIAMS, C., SHARPLES, J., MAHAFFEY, C. & RIPPETH, T. 2013. Wind-driven nutrient pulses to the subsurface chlorophyll maximum in seasonally stratified shelf seas. *Geophysical Research Letters*, 40, 5467-5472.
- WILLIAMS, P. J. L. B. 1998. The balance of plankton respiration and photosynthesis in the open oceans. *Nature*, 394, 55-57.
- WILLIAMS, P. J. L. B. & BOWERS, D. G. 1999. Regional Carbon Imbalances in the Oceans. *Science*, 284, 1735-1735.
- WOOLF, D. K. & THORPE, S. A. 1991. Bubbles and the air-sea exchange of gases in nearsaturation conditions. *Journal of Marine Research*, 49, 435-466.
- WU, Y., PLATT, T., TANG, C. C. L., SATHYENDRANATH, S., DEVRED, E. & GU, S. 2008. A summer phytoplankton bloom triggered by high wind events in the Labrador Sea, July 2006. *Geophysical Research Letters*, 35.
- ZHAI, L., PLATT, T., TANG, C., SATHYENDRANATH, S. & WALNE, A. 2013. The response of phytoplankton to climate variability associated with the North Atlantic Oscillation. *Deep Sea Research Part II: Topical Studies in Oceanography*, 93, 159-168.

## 6 Appendix A – Biofouling

Figure 1a shows that  $c(\text{O}_2)$  increased throughout the water column in the last month of the time series. At the surface,  $c(\text{O}_2)$  reached values that were higher than in the rest of the year, and also showed increases at depths where it had been stable for the rest of the year. A careful analysis of this period was therefore carried out in order to understand the reason for this phenomenon.

The presence of high  $c(\text{O}_2)$  values near the surface was considered first. There was an anomalous increase in  $c(\text{O}_2)$  that was particularly visible near the deep chlorophyll maximum, where  $c(\text{O}_2)$  reaches  $343 \mu\text{mol kg}^{-1}$  (Figure 1). At the same time there was a discrepancy between the data collected during the ascent and the

descent of each glider dive. Figure A.1 shows the concentration at 11 m as measured during descents and ascents. After 11<sup>th</sup> August,  $c(\text{O}_2, 11 \text{ m})$  in the ascents is higher than in the descents. The magnitude of this difference increased over time, especially in the first metres of the water column down to the deep chlorophyll maximum (data not shown). However, during the night  $c(\text{O}_2)$  values measured during the ascents and descents matched again (Figure A.1c).

Sunlight seems therefore to be a possible factor causing this difference. This was possibly related to the different angle that the optode had with respect to the incident light according to the direction of the glider (Figure A.2). The foil was virtually parallel to the surface in the ascents and more angled with respect to the incident light during the descents. This means that the probe was hit directly by the light when the glider went towards the surface, whereas it received less light when it went towards the deep. This was not enough to explain why the two phases of the dives are different in the last month of measurements, because otherwise this phenomenon would have been visible throughout the whole time series. There must have been therefore a new factor that, interacting with the foil and with the light, caused the difference between ascents and descents in this part of the year. The increasing mismatch between phases (Figure A.1 a-c) also showed that this new factor had a growing influence on the sensor over time.

In the last month of the dataset there was also an increase in  $c(\text{O}_2)$  in the otherwise overall stable minimum  $c(\text{O}_2)$ ,  $c_{\min}(\text{O}_2)$  (Figure 14b). Being distant from the surface and from the euphotic depth  $z_{\text{eup}}$ , this deep water mass was expected to be stable because it was not exposed to the big perturbations due to air-sea exchange and biological productivity. After 11<sup>th</sup> August there was a fast and un-interrupted increase of  $c_{\min}(\text{O}_2)$  that reached  $226 \mu\text{mol kg}^{-1}$ . Considering that this sharp increase in  $c(\text{O}_2)$  at depth began at the same time as the discrepancy between ascents and descents (on 11<sup>th</sup> August), these events were considered to be caused by the same factor. The descents seem to be less affected, while ascents show obviously unrealistic values during the day (Figure A1a). However, descents still show an increasing pattern over time, showing that data cannot be used despite the direction of the glider movement.

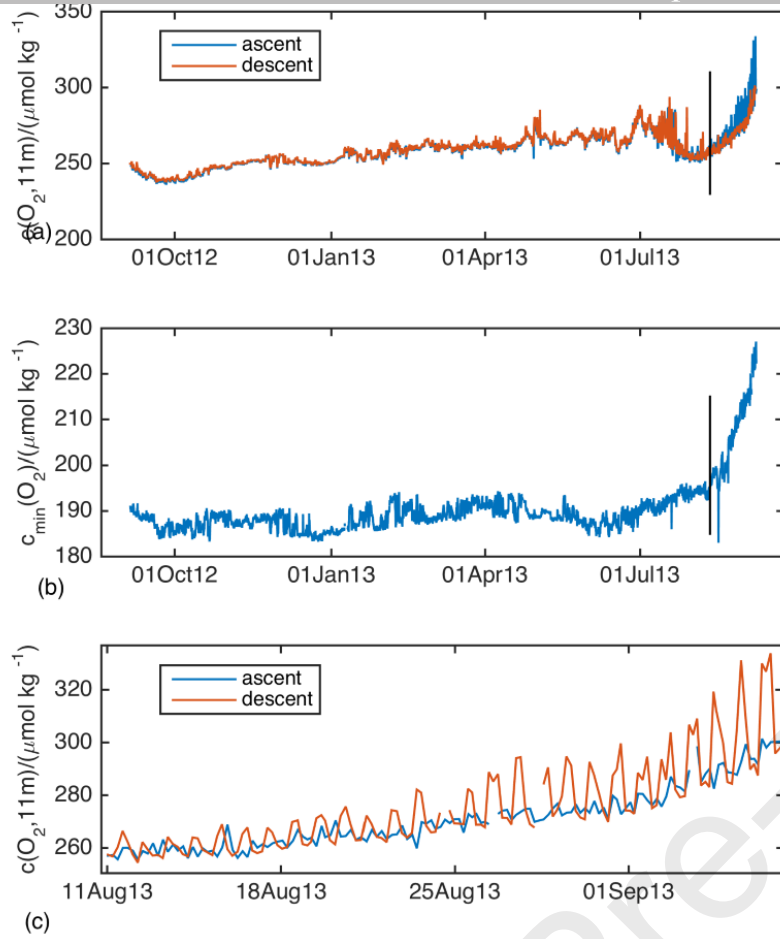


Figure A.1 (a) Oxygen concentration at the 11 m horizon during the ascending phase (blue) and descending (red) phase of glider dives; (b) Minimum oxygen concentration (if measured within the boundaries of Intermediate Water). In both (a) and (b) the black vertical line marks the date of August 11<sup>th</sup>, when the bias due to biofouling starts formally. (c) focus from panel (a) during the biofouling-affected period showing the difference between ascents and descents that mismatched during daytime and matched again at night.

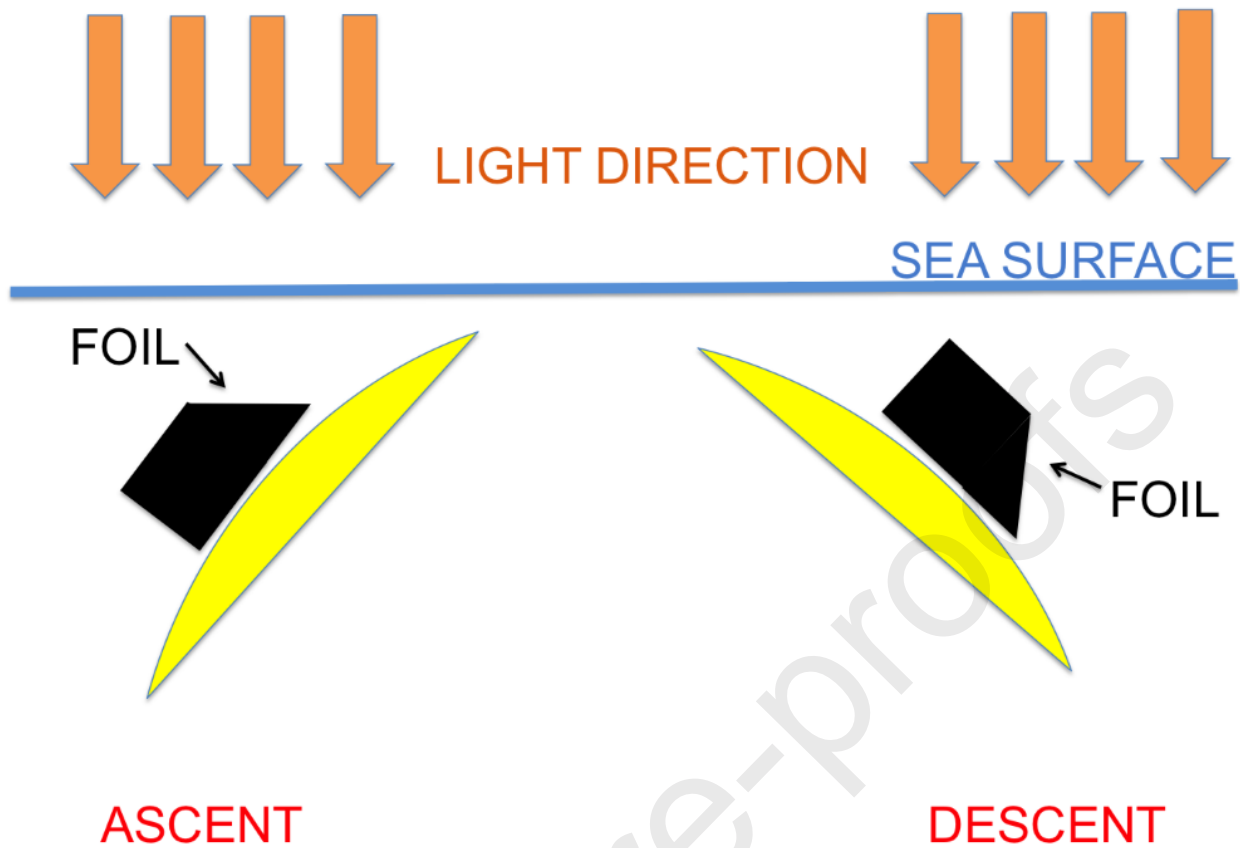


Figure A.2 Scheme of the position of the foil of the optode with respect to the surface and to the incident light in the ascents and descents of each dive.

Biofouling of the foil was the most likely factor behind the phenomena just described. It probably developed on top of the optode foil after the beginning of the productive period, when chlorophyll *a* concentration at the top of the water column was higher than in the rest of the year (beginning of July 2013, Figure 2h). This is usually a proxy for the presence of high phytoplankton biomass, which makes it plausible that phytoplankton started to grow into a biofilm on the foil. The algae, producing more  $O_2$  when exposed to direct and stronger light (during ascents), would have caused the difference between profiles in different phases.  $O_2$  produced by the biofilm would have given high  $c(O_2)$  readings not reflecting the actual  $c(O_2)$  in the water column. Furthermore, the amount of gas released by the biofilm would have been proportional to its biomass – the growth of the biofilm would explain why there was an increase in the difference between phases, of  $c(O_2, \text{surface})$  and of  $c_{\min}(O_2)$ . At the recovery of the glider, all the sensors were covered by a green biofilm (Stephen Woodward, personal communication). The data collected after 11<sup>th</sup> August are therefore considered not valid for the scope of this study. As a lesson learnt, datasets should be checked, especially when missions last for several months in productive areas; discrepancies between ascents and descents appearing during the day and disappearing during the night, and the increase of values in deep water masses that are usually stable should be signs to look for to spot the possible presence of biofouling and question the validity of the data.

Biofouling is a well-known problem in oceanographic measurements (Tosteson et al., 1982; Manov et al., 2004; Delauney et al., 2010). It has been advocated in previous studies to be the cause of drift in optical sensors mounted on both moorings (e.g., Kinkade, 2001; Manov et al., 2004; Heupel et al., 2008) and gliders (e.g., Nicholson et al., 2008; Cetinić et al., 2009; Krahmann et al., 2011). The interest of the scientific community for the new solutions that can reduce the biofouling (e.g., Manov et al., 2004; Whelan and Regan, 2006; Delauney et al., 2010; Lobe et al., 2010; Lobe, 2015) is a clear evidence of the importance of this problem for oceanographic observations. The research is particularly active in the glider-users community since the biofouling can also affect the flight performances of these vehicles (Krahmann et al., 2011; Moline and Went, 2011). Possible options include installation of wipers for mechanical removal of the fouling and special foul releasing coating to reduce biofouling settlement and growth; however, hydrodynamic must be taken into account not to impact performances (Lobe, 2015).

CETINIĆ, I., TORO-FARMER, G., RAGAN, M., CARL OBERG, C. & JONES, B. H. 2009. Calibration procedure for Slocum glider deployed optical instruments. *Opt. Express*, 17, 15420-15430.

DELAUNEY, L., COMPERE, C. & LEHAITRE, M. 2010. Biofouling protection for marine environmental sensors. *Ocean Science*, 6, 503-511.

HEUPEL, M. R., REISS, K. L., YEISER, B. G. & SIMPFENDORFER, C. A. 2008. Effects of biofouling on performance of moored data logging acoustic receivers. *Limnology and Oceanography: Methods*, 6, 327-335.

KRAHMANN, G., KANZOW, T., KARSTENSEN, J. & SCHLUNDT, M. 2011. Results from a Glider Swarm Experiment near Cape Verde. [http://eprints.uni-kiel.de/12248/1/EGO\\_2011\\_-\\_Gerd\\_Krahmann.pdf](http://eprints.uni-kiel.de/12248/1/EGO_2011_-_Gerd_Krahmann.pdf)

LOBE, H., 2015, October. Recent advances in biofouling protection for oceanographic instrumentation. In *OCEANS 2015-MTS/IEEE Washington* (pp. 1-4). IEEE.

MANOV, D. V., CHANG, G. C. & DICKEY, T. D. 2004. Methods for reducing biofouling of moored optical sensors. *Journal of Atmospheric and Oceanic Technology*, 21, 958-968.

MOLINE, M. A. & WENDT, D. 2011. Evaluation of glider coatings against biofouling for improved flight performance. DTIC Document.

NICHOLSON, D., EMERSON, S. & ERIKSEN, C. C. 2008. Net community production in the deep euphotic zone of the subtropical North Pacific gyre from glider surveys. *Limnology and Oceanography*, 53, 2226-2236.

THOMPSON, A.F., A. LAZAR, C.E. BUCKINGHAM, A.C. NAVEIRA GARABATO, G.M. DAMERELL & K.J. HEYWOOD, 2016. Open-ocean submesoscale motions: A full seasonal cycle of mixed layer instabilities from gliders. *J. Phys. Oceanogr.*, 46, 1285-1307.

TOSTESON, T. R., ZAIDI, B. R., REVUELTA, R., IMAN, S. H., AXTMAYER, R. W., DE VORE, D., BALLANTINE, D. L., SASSCER, D. S., MORGAN, T. O. & RIVERA, C. 1982. OTEC biofouling, corrosion, and materials study from a moored platform at Punta Tuna, Puerto Rico. II. Microbiofouling. *Ocean science and engineering*.

WHELAN, A. & REGAN, F. 2006. Antifouling strategies for marine and riverine sensors. *J. Environ. Monit.*, 8, 880-886.



## Appendix B – Method Sensitivity

In order to test the sensitivity of the method and determine the uncertainties associated with the  $N$  estimates discussed above, we assessed the influence of different parameters and choices made.

If glider ascents are used in the calculations, the mean  $N$  is 2 % greater than calculated with descents (Figure A.3). However, considering that the optode was influenced in a different way during ascents and descents, this calculation could have been potentially influenced by the initial growth of biofouling at the end of the dataserries.

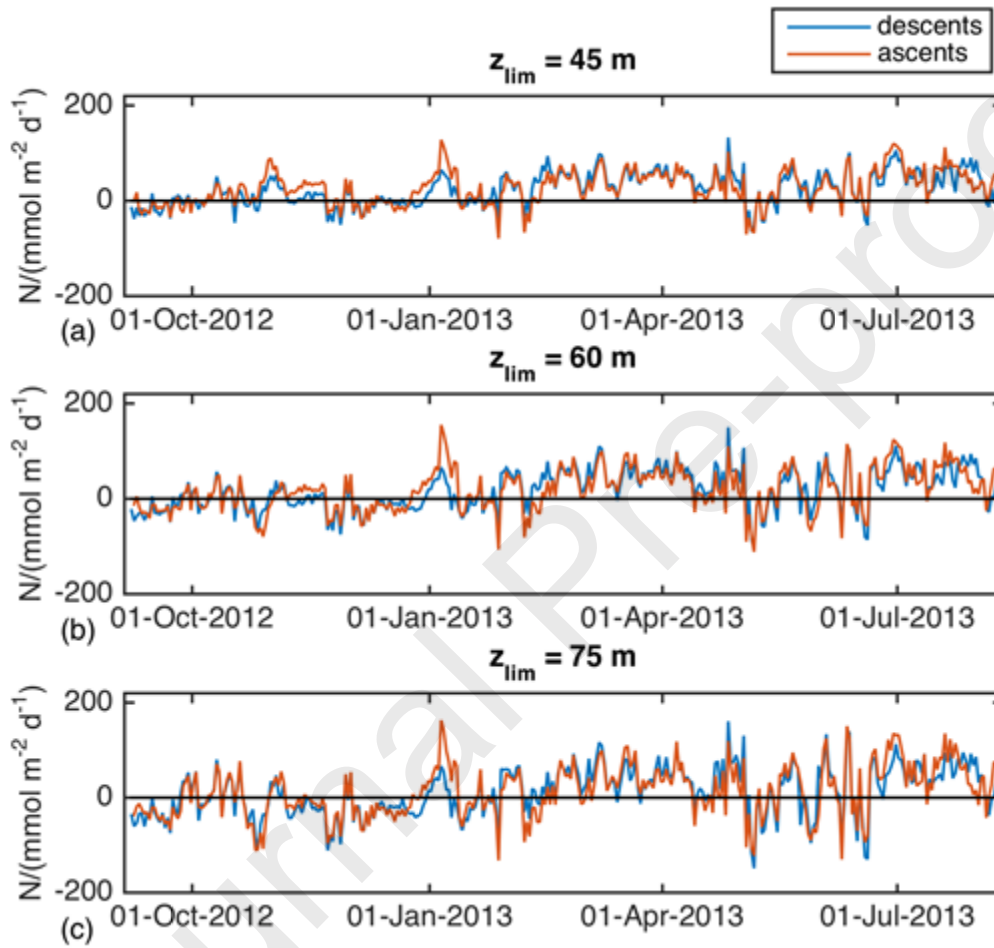


Figure A.3 Net community production time series measured above (a) 45 m, (b) 60 m and (c) 75 m using descents (blue lines) and ascents (red lines) from each glider dive.

Since the mean and standard deviation of  $z_{eup}$  were 60 m and 15 m respectively, mean and total cumulative  $N$  were recalculated using 45 m and 75 m as  $z_{lim}$  (Table A.1 **Error! Reference source not found.**). These shallower and deeper  $z_{lim}$  were considered respectively an underestimation and overestimation of  $N$  in the euphotic zone. The shallower  $z_{lim}$  measure in fact only the very productive top layer of the water disregarding the respiration happening deeper down. A deeper  $z_{lim}$  based on the deepest  $z_{eup}$ , instead, accounts for all the respiration happening in the deeper parts when the euphotic layer is thinner. The mean difference between  $N$

determined using  $z_{lim} = 45, 60$  and  $75$  m was used as a measure of the uncertainty associated with  $N_{cup}$  ( $\pm 0.5$  mmol m<sup>-2</sup> d<sup>-1</sup>,  $\pm 2.1$  mol m<sup>-2</sup>,  $\pm 30\%$ ).

Table A.1 Net community production mean, standard deviation and total sum calculated above 45 m, 60 m and 75 m.

| $z_{lim}$ / m | Mean $N$ /<br>mmol m <sup>-2</sup> d <sup>-1</sup> | Standard deviation $N$ /<br>mmol m <sup>-2</sup> d <sup>-1</sup> | Total $N$ /<br>mol m <sup>-2</sup> |
|---------------|--|--|------------------------------------|
| 45            | 24.7   | 35.1   | 8.4                                |
| 60            | 19.0   | 43.0   | 6.5                                |
| 75            | 12.1   | 52.7   | 4.1                                |

Another test was performed to assess the sensitivity of the method to the 7-day length of the averaging bins.  $N$  was recalculated binning over 1 day, 3 days, 5 days, 7 days, 9 days, 11 days, 13 days and 15 days (Table A.2). The maximum change with respect to the values averaged over 7-day bins was obtained using 15-day bins, which increased mean  $N$  by 6.5 %. This value was one order of magnitude smaller than the uncertainty related to changes in  $z_{lim}$  so was ignored in the error budget. Therefore, the uncertainty of  $\pm 30\%$  estimated from the choice of  $z_{lim}$  was used, as the uncertainty introduced by different bin lengths was considered to be negligible in comparison.

Table A.2 Mean values of the net community production time series obtained by averaging individual estimates between consecutive profiles over different bin lengths.

| Mean $N$ (mmol m <sup>-2</sup> d <sup>-1</sup> in O <sub>2</sub> equivalents) for time series obtained averaging over... |        |        |        |        |         |         |         |
|--|--------|--------|--------|--------|---------|---------|---------|
| 1 day  | 3 days | 5 days | 7 days | 9 days | 11 days | 13 days | 15 days |
| 19.0   | 18.9   | 18.9   | 19.0   | 19.2   | 19.6    | 20.0    | 20.3    |

### Supplementary material – Calibration of the gliders

The first two missions were calibrated using CTD casts from the cruises that visited the site to deploy and recover the gliders. These casts were performed when the ship was close to the profiling gliders (figure 2.13a-b). SG599 was instead calibrated using CTD casts from three different cruises. Apart the deployment and recovery cruises, another one (JC087) visited the site in the middle of the mission (locations in figure 2.13c). Seven different calibrations were then performed during the study, whose details are listed in Table Sup.1. The linear calibration equations calculated for each mission are compared in Figure Sup.1.

Table Sup.1 CTD casts and glider dives used per each calibration,  $r^2$  value of the regression between the CTD cast and the glider dive used, and calibration equation using  $TPhaseCoef_0$  and  $TPhaseCoef_1$  obtained by the regression and uncertainty associated to the calibration.

| Seaglider mission | CTD     | $r^2$ | Calibration equation<br>$C = \phi_{cal}, T = \phi_{TC}$<br>$\pm$ uncertainty ( $\phi_{cal}$ unit) | Uncertainty<br>$\pm \mu\text{mol kg}^{-1}$ |
|-------------------|---------|-------|---|--|
| SG566             | D381    | 0.998 | $C = 0.9341 \times T - 0.0597$<br>$\pm 0.11$  | 1.84                                       |
|                   | CE13001 | 0.998 | $C = 0.9563 \times T - 1.3937$<br>$\pm 0.13$  | 2.80                                       |
|                   |         |       |   |  |
| SG502             | CE13001 | 0.996 | $C = 0.9796 \times T - 1.4487$<br>$\pm 0.12$  | 2.23                                       |
|                   | JC085   | 0.999 | $C = 0.9464 \times T - 1.5059$<br>$\pm 0.10$  | 1.73                                       |
|                   |         |       |   |  |
| SG599             | JC085   | 0.998 | $C = 0.9122 \times T + 0.1628$<br>$\pm 0.14$  | 2.21                                       |
|                   | JC087   | 0.999 | $C = 0.9418 \times T - 1.1863$<br>$\pm 0.11$  | 2.30                                       |
|                   | JC090   | 0.958 | $C = 0.9109 \times T + 1.0022$<br>$\pm 0.26$  | 4.98                                       |

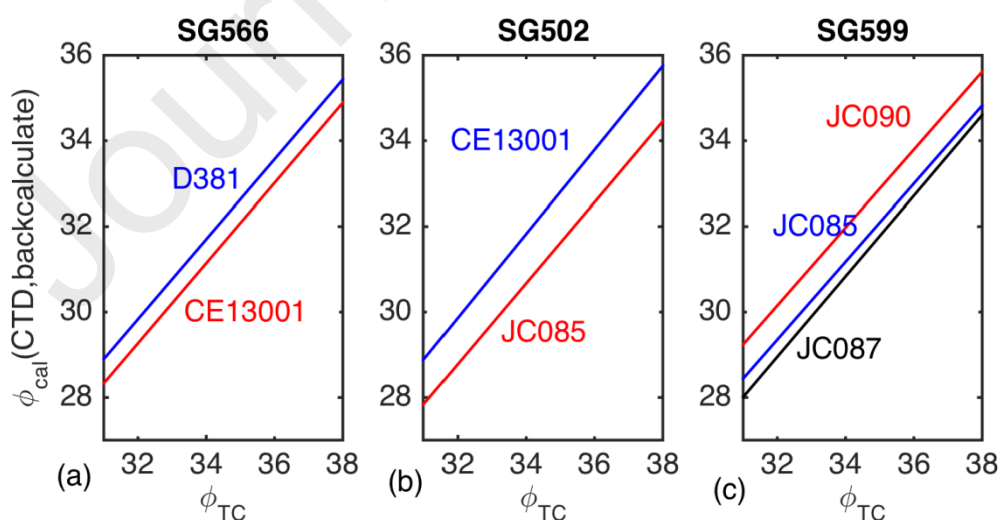


Figure Sup.1 Calibration linear equations for the beginning (blue) and the end (red) of each glider mission for (a) SG566, (b) SG502 and (c) SG599. In (c) a third calibration done in the middle of the mission is also shown in black. The name of the cruises of the calibrating CTD casts is also shown.

The calibration equation changed for each profile considering a linear drift over time. For each glider mission, a value for  $C_0$  and a value for  $C_1$  were calculated at the beginning of the mission ( $C_{0(s)}$ ,  $C_{1(s)}$ ) and at the end of the mission ( $C_{0(e)}$ ,  $C_{1(e)}$ ). These values were considered valid only for the profiles at  $t_s$  and  $t_e$  respectively. For any other profile at  $t_x$ ,  $C_{0(x)}$  and  $C_{1(x)}$  were measured assuming a linear drift as follows:

$$C_{0(t)} = [(C_{0(e)} - C_{0(s)} / (t_e - t_s)] * t_x + [(C_{0(e)} * t_s) - (C_{0(s)} * t_e)] / (t_e - t_s)$$

$$C_{1(t)} = [(C_{1(e)} - C_{1(s)} / (t_e - t_s)] * t_x + [(C_{1(e)} * t_s) - (C_{1(s)} * t_e)] / (t_e - t_s)$$

Net community oxygen production derived from Seaglider deployments at the Porcupine Abyssal Plain site (PAP; northeast Atlantic) in 2012-13

U. Binetti<sup>1,2</sup>, J. Kaiser<sup>2</sup>, G. M. Damerell<sup>2</sup>, A. Rumyantseva<sup>3</sup>, A.P. Martin<sup>4</sup>, S. Henson<sup>4</sup>, K. J. Heywood<sup>2</sup>

<sup>1</sup>Centre for Environment, Fisheries and Aquaculture Science, Lowestoft, UK

[Umberto.binetti@cefas.co.uk](mailto:Umberto.binetti@cefas.co.uk), [u.binetti@uea.ac.uk](mailto:u.binetti@uea.ac.uk)

Umberto Binetti, Cefas Laboratories, Pakefield Road, Lowestoft, UK NR33 0HT.

<sup>2</sup>Centre for Ocean and Atmospheric Sciences, School of Environmental Sciences, University of East Anglia, Norwich, United Kingdom

<sup>3</sup>School of Ocean and Earth Sciences, University of Southampton, Southampton, UK

<sup>4</sup>National Oceanography Centre, Southampton, UK

## Highlights

- The area analysed is autotrophic over an annual cycle
- Marine net biological production is estimated at  $19 \text{ mmol m}^{-2} \text{ d}^{-1}$  in  $\text{O}_2$  equivalents with a total production of  $6.4 \text{ mol m}^{-2} \text{ O}_2$  equivalent
- Initiation of phytoplankton blooms in different time of the year follow dynamics described by up to three theories (Critical Depth Hypothesis, Critical Turbulence Hypothesis, Heat-flux Hypothesis).
- Water is oxygen undersaturated during the whole winter period.

Net community oxygen production derived from Seaglider deployments at the Porcupine Abyssal Plain site (PAP; northeast Atlantic) in 2012-13

U. Binetti<sup>1,2</sup>, J. Kaiser<sup>2</sup>, G. M. Damerell<sup>2</sup>, A. Rumyantseva<sup>3</sup>, A.P. Martin<sup>4</sup>, S. Henson<sup>4</sup>, K. J. Heywood<sup>2</sup>

<sup>1</sup>Centre for Environment, Fisheries and Aquaculture Science, Lowestoft, UK

[Umberto.binetti@cefas.co.uk](mailto:Umberto.binetti@cefas.co.uk), [u.binetti@uea.ac.uk](mailto:u.binetti@uea.ac.uk)

Umberto Binetti, Cefas Laboratories, Pakefield Road, Lowestoft, UK NR33 0HT.

<sup>2</sup>Centre for Ocean and Atmospheric Sciences, School of Environmental Sciences, University of East Anglia, Norwich, United Kingdom

<sup>3</sup>School of Ocean and Earth Sciences, University of Southampton, Southampton, UK

<sup>4</sup>National Oceanography Centre, Southampton, UK

The authors declare no conflict of interest.